Imaging the crustal structure of the Central Iberian Zone (Variscan Belt): The ALCUDIA deep seismic reflection transect

D. Martínez Poyatos,[1] R. Carbonell,[2] I. Palomeras,[2,3] J. F. Simancas,[1] P. Ayarza,[4] D. Martí,[2] A. Azor,[1] A. Jabaloy,[1] P. González Cuadra,[5] R. Tejero,[6] L. M. Martín Parra,[5] J. Matas,[5] F. González Lodeiro,[1] A. Pérez-Estaún,[2] J. L. García Lobón,[5] and L. Mansilla[7]

Received 14 July 2011; revised 20 April 2012; accepted 26 April 2012; published 15 June 2012.

[1] ALCUDIA is a 230 km long, vertical incidence deep seismic reflection transect acquired in spring 2007 across the southern Central Iberian Zone (part of the pre-Mesozoic Gondwana paleocontinent) of the Variscan Orogen of Spain. The carefully designed acquisition parameters resulted in a 20 s TWTT deep, 60–90 fold, high-resolution seismic reflection transect. The processed image shows a weakly reflective upper crust (the scarce reflectivity matching structures identified at surface), a thick, highly reflective and laminated lower crust, and a flat Moho located at 10 s TWTT (∼30 km depth). The transect can be divided into three segments with different structural styles in the lower crust. In the central segment, the lower crust is imaged by regular, horizontal and parallel reflectors, whereas in the northern and southern segments it displays oblique reflectors interpreted as an important thrust (north) and tectonic wedging involving the mantle (south). The ALCUDIA seismic image shows that in an intracontinental orogenic crust, far from the suture zones, the upper and lower crust may react differently to shortening in different sectors, which is taken as evidence for decoupling. The interpreted structures, as deduced from surface geology and the seismic image, show that deformation was distributed homogeneously in the upper crust, whereas it was concentrated in wedge/thrust structures at specific sectors in the lower crust. The seismic image also shows the location of late Variscan faults in spatial association with the lower crustal thickened areas.

Citation: Martínez Poyatos, D., et al. (2012), Imaging the crustal structure of the Central Iberian Zone (Variscan Belt): The ALCUDIA deep seismic reflection transect, *Tectonics*, *31*, TC3017, doi:10.1029/2011TC002995.

1. Introduction

[2] Lithospheric scale and orogenic processes are linked to the Earth's interior dynamics. The way they are linked is a topic of current research since the early 1970s. To unravel these links it is imperative to establish the structure and deformation mechanisms of the lithosphere, by combining surface geology information with indirect geophysical data on the hidden part of the lithosphere.

[3] A wealth of knowledge in crustal and lithospheric architecture has been developed through deep seismic reflection profiling (e.g., COCORP [*Cook et al.*, 1979; *Brown et al.*, 1983], DEKORP [*DEKORP Research Group*, 1985, 1988; *Onken et al.*, 2000], LITHOPROBE [*Cook et al.*, 1999], URSEIS/ESRU [*Echtler et al.*, 1996; *Juhlin et al.*, 1998; *Tryggvason et al.*, 2001]), a powerful tool to study lithospheric plate interiors. The recent technological developments in acquisition and processing techniques, along with the new modeling and interpretation strategies, have increased the resolution of this type of information.

[4] Up to now deep seismic imaging has been mainly addressed to orogenic sutures, in an effort to understand the history and behavior of colliding plates. Thus, much has been learnt about the characteristics of deformation in the edges of old and present continents, where an important part of the deformation is resolved by imbrication of the lithosphere in plate boundaries. Conversely, less interest has been paid to lithospheric scale processes affecting intracontinental areas (e.g., COCORP [*Cook et al.*, 1979; *Brown et al.*, 1983]),

[1]Departamento de Geodinámica, Facultad de Ciencias, Universidad de Granada, Granada, Spain.
[2]Instituto de Ciencias de la Tierra "Jaume Almera," CSIC, Barcelona, Spain.
[3]Department of Earth Science, Rice University, Houston, Texas, USA.
[4]Departamento de Geología, Universidad de Salamanca, Salamanca, Spain.
[5]Instituto Geológico y Minero de España, Madrid, Spain.
[6]Departamento de Geodinámica, Universidad Complutense de Madrid, Madrid, Spain.
[7]Escuela Politécnica Universitaria de Almadén, Universidad de Castilla-La Mancha, Almadén, Spain.

Corresponding author: D. Martínez Poyatos, Departamento de Geodinámica, Facultad de Ciencias, Universidad de Granada, E-18071 Granada, Spain. (djmp@ugr.es)

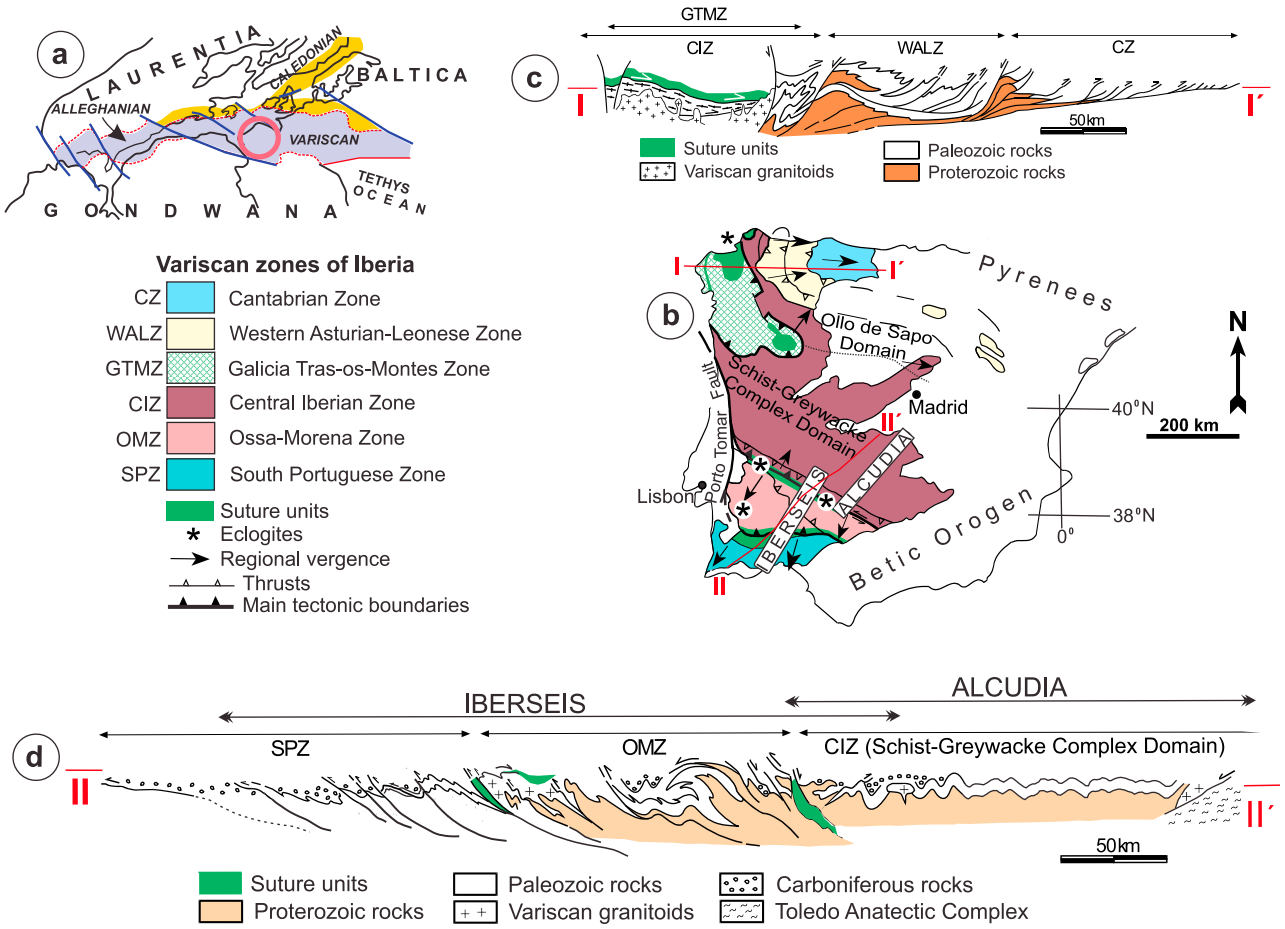

Figure 1. Location and tectonic setting of the European Variscides in Iberia. (a) Sketch of the Alleghanian-Variscan Orogen. The location of the Iberian Massif is denoted by the red circle at the edge of Gondwana. (b) Main zonal division of the Variscan Iberian Massif. The IBERSEIS and ALCUDIA deep seismic reflection transects are located. (c) Geological cross section of northern Iberia (adapted from *Pérez-Estaún et al.* [1991]). (d) Complete cross section incorporating the IBERSEIS and ALCUDIA transects. See auxiliary material for a larger version of this image.

where geological processes have rarely exhumed deep rocks to surface and where there is little control on the structure below 5–10 km depth.

[5] The ALCUDIA deep seismic profile was acquired in spring 2007 across the southern Central Iberian Zone (CIZ) (Figure 1) (see the auxiliary material for larger images of all figures).[1] This region is part of the Variscan/Alleghanian Orogen, which resulted from the Late Paleozoic collision between two continents, Laurentia/Baltica and Gondwana (Figure 1). Surface geology along most of the ALCUDIA transect shows part of the Gondwana paleocontinent, here characterized by limited offset faults and upright folds [e.g., *Díez Balda et al.*, 1990], which allow an ambiguous control of the crustal structure at depth. Therefore, only the integration of geological field studies with indirect geophysical methods can shed some light on the structure of the Central Iberian lithosphere. The main goal of the ALCUDIA seismic transect was to image the structure and to unravel the geodynamic evolution of an old intracontinental orogenic region, far from known sutures, and with no evidence of weak, high-strain zones within the crust.

[6] The SW Iberian transect formed by the integration of the IBERSEIS [*Simancas et al.*, 2003; *Carbonell et al.*, 2004; *Palomeras et al.*, 2009] and the ALCUDIA seismic profiles provides a unique and complete section of the Variscan Orogen in the southern Iberian Massif (Figure 1). It adds to previous studies performed in the northern Iberian Massif (e.g., ESCIN [*Pérez-Estaún et al.*, 1991, 1994, 1995; *Pulgar et al.*, 1995; *Martínez Catalán et al.*, 1995; *Ayarza et al.*, 1998, 2004]), as well as in central Europe (e.g., BIRPS [*Klemperer and Matthews*, 1987; *Freeman et al.*, 1988], ECORS [*ECORS Pyrenean Team*, 1988], DEKORP [*Onken et al.*, 2000]), and in the Urals [*Echtler et al.*, 1996; *Carbonell et al.*, 1996, 1998, 2000; *Juhlin et al.*, 1998; *Tryggvason et al.*, 2001; *Friberg et al.*, 2002]. The IBERSEIS profile provided a model of the Variscan structures across three tectonic zones bounded by two sutures exposed in SW Iberia (Figure 1). The ALCUDIA profile shows how the internal architecture of the Variscan Orogen extends towards the interior of the Iberian Massif, within the

[1]Auxiliary materials are available in the HTML. doi:10.1029/2011TC002995.

Gondwana paleosupercontinent. The ALCUDIA image constrains the structural styles at different crustal levels, as well as the mechanisms that tend to keep a constant crustal thickness.

2. Geological Setting

2.1. Overview

[7] The ALCUDIA seismic profile images a lithospheric section of the Iberian Massif, which constitutes the largest outcrop of the Late Paleozoic Variscan/Alleghanian Orogen in western Europe (Figure 1). This orogen resulted from the subduction and closure of the Rheic Ocean that separated the Laurentia/Baltica and Gondwana continents during the Early Paleozoic (Ordovician to Devonian). Subsequent collision in Devonian-Carboniferous times amalgamated these continents along with intervening minor oceanic domains (e.g., Rheno-Hercynian) and elongated continental domains (e.g., Armorica) [*Franke*, 2000; *Matte*, 2001]. Later opening of the Atlantic Ocean and Alpine reworking dismembered the orogen into several portions that now crop out in western Europe, northwest Africa and northeast America.

[8] The Iberian Massif (Figure 1) exposes a complete section of the Variscan Belt, from the external South Portuguese Zone (SPZ) in the south, through more internal zones [Ossa-Morena Zone (OMZ), Central Iberian Zone (CIZ), Galicia-Tras-os-Montes Zone and West-Asturian Leonese Zone], to the counterpart external Cantabrian Zone in the north [*Lotze*, 1945; *Julivert et al.*, 1972]. The Central Iberian, West-Asturian Leonese, and Cantabrian zones are continental domains that formed part of a wide passive margin along northern Gondwana prior to the Variscan orogeny. The Galicia-Tras-os-Montes Zone is an unrooted complex zone that partially overlies the northwestern CIZ, and includes, among others, ophiolite slices representing remnants of the Rheic Ocean [*Arenas et al.*, 2007]. The OMZ is commonly interpreted as a continental domain that rifted (and drifted to some extent) from Gondwana (i.e. the CIZ) in the Early Paleozoic [*Matte*, 2001; *Robardet*, 2002; *Gómez-Pugnaire et al.*, 2003]. Subsequent collision between these two zones resulted in the suture unit known as the Badajoz-Córdoba Shear Zone [*Burg et al.*, 1981] or Central Unit [*Azor et al.*, 1994]. Some controversy concerns the likely suture between the OMZ and the SPZ [*Azor et al.*, 2008], the latter probably representing a part of the Avalonia (Laurentia) paleocontinent [*Tait et al.*, 2000; *Braid et al.*, 2011].

[9] The CIZ has been classically subdivided into two domains (Figure 1) [e.g., *Díez Balda et al.*, 1990]: the northern one (Ollo de Sapo Domain), characterized by Ordovician augen gneisses and Variscan recumbent folds; and the southern one (Schist-Greywacke Complex Domain), with a simpler structure characterized by large NW-SE trending upright folds and faults. The ALCUDIA seismic transect cuts, across a NE-SW section, the Schist-Greywacke Complex Domain. The transect was designed to be perpendicular to the main trend of the geological contacts and structures (Figure 2). The southern end of the transect coincides with the Central Unit, thus reaching the boundary with the OMZ.

[10] The Variscan tectonic evolution in SW Iberia can be summarized as follows [e.g., *Simancas et al.*, 2003]: (1) Devonian compression (D1, 390–360 Ma): subduction/collision along the OMZ/CIZ boundary, and related recumbent folding in the OMZ and in the southernmost CIZ; (2) Mississippian extension (D2, 360–330 Ma): normal faulting, basin filling and mafic magmatism in the SPZ, OMZ and in the southernmost CIZ; (3) Renewed Pennsylvanian compression (D3, 330–310 Ma): basin inversion and upright folding; (4) Late Pennsylvanian-Permian extension (D4, 310–280 Ma): localized normal faulting and late-orogenic granitic magmatism, without significant sedimentary basin development.

[11] The main geological features of the Schist-Greywacke Complex Domain include (Figure 2): (1) a thick Neoproterozoic-Lower Cambrian synorogenic sedimentary succession related to the denudation of a Cadomian orogenic belt, (2) an Ordovician to Devonian marine siliciclastic succession related to a passive-margin continental platform, and (3) a thick Mississippian syn-orogenic sedimentary succession (the Pedroches Flysch, located in the southernmost CIZ) related to D2 extensional tectonics. The whole sequence was affected by D3 Pennsylvanian upright folding at very low-grade metamorphic conditions, as well as by local D4 late Variscan extensional tectonics. A more detailed geological description follows below.

2.2. The OMZ/CIZ Suture

[12] The Central Unit separating the OMZ and the CIZ is a ≥5 km thick crustal sheet that dips towards the northeast [*Azor et al.*, 1994] (Figure 2). It consists of metasediments, Ordovician orthogneisses and minor lenses of (retroeclogitic) amphibolites, intensely sheared and metamorphosed in the earliest Carboniferous [*Ordóñez Casado*, 1998; *Pereira et al.*, 2010]. Some of the amphibolites are Early Paleozoic [*Ordóñez Casado*, 1998] and have an oceanic geochemical signature [*Gómez-Pugnaire et al.*, 2003]. The Matachel Fault is a brittle, north-dipping low-angle normal fault that bounds the Central Unit to the north (Figure 2). The Central Unit was imaged by the IBERSEIS seismic reflection profile (Figure 1) [*Simancas et al.*, 2003] as a northeast dipping reflective wedge in the upper crust. This wedge merges downdip with a mid-crustal detachment, while its top is truncated by the Matachel Fault. Shearing and faulting of the Central Unit occurred during the D2 Mississippian extension, which contributed to its exhumation [*Azor et al.*, 1994].

2.3. Lithostratigraphy

[13] The oldest outcropping rocks in the OMZ and in the southernmost CIZ are Late Neoproterozoic in age and consist in >3000 m of graphite-rich schists, slates and metagreywackes with black quartzites, amphibolites and minor marble intercalations (Serie Negra). In some areas, the Serie Negra is overlain by the Vendian-Lower Cambrian, volcanoclastic Malcocinado Formation. To the north of the Pedroches Batholith (Figure 2), the oldest outcropping rocks are those of the Vendian to Lower Cambrian Schist-Greywacke Complex. This complex is termed Alcudian succession here and subdivided by unconformities into Lower Alcudian, Upper Alcudian and Pusian (Figure 2). Total thickness of the Alcudian succession can exceed 10,000 m, though it varies by sectors according to different authors. The Lower Alcudian succession is a monotonous sequence of slates and greywackes with some conglomerates and minor volcanic rocks. The overlying successions are lithologically more varied and composed by prevailing slates with intercalations of black shales, conglomerates, sandstones, limestones,

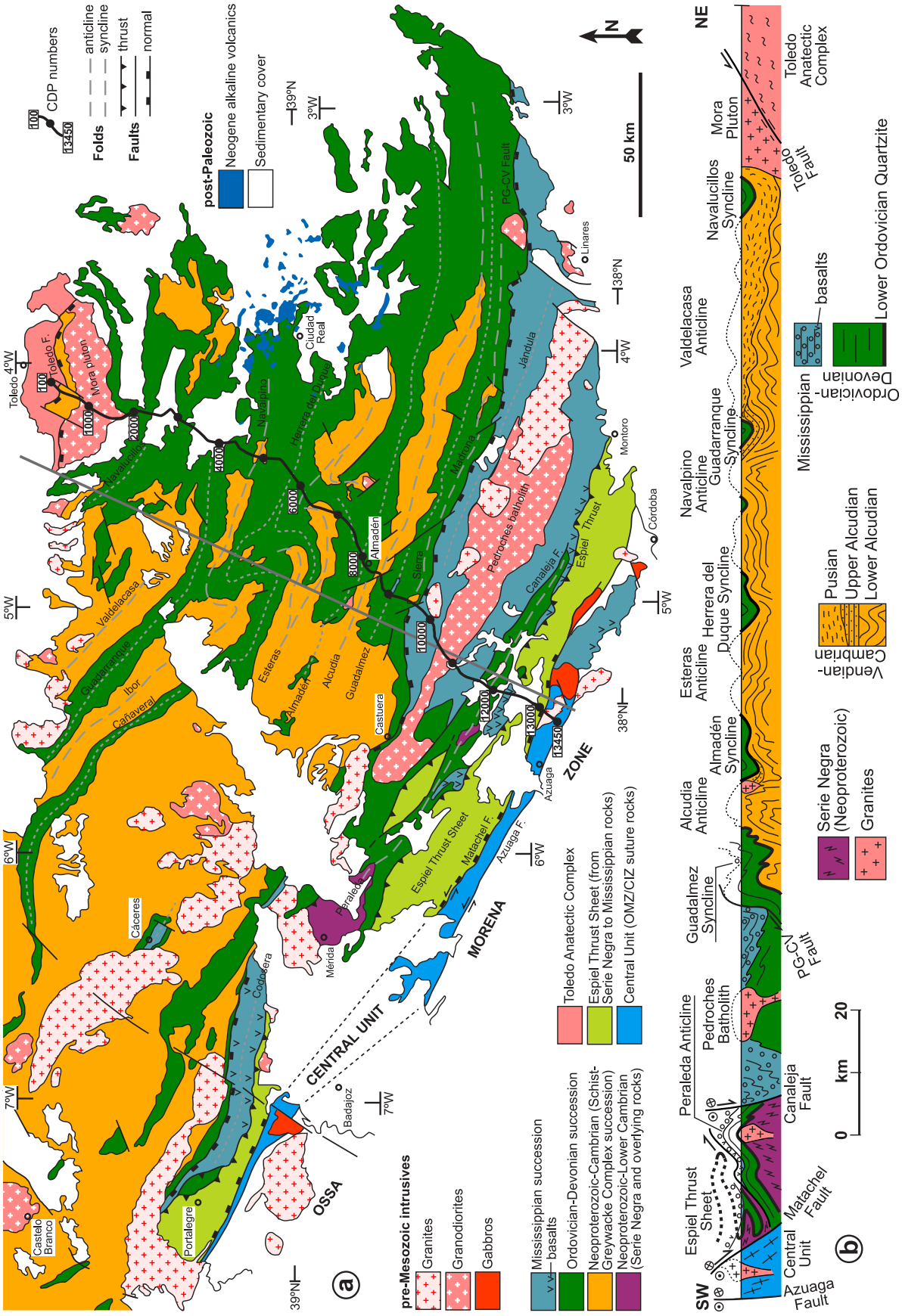

Figure 2. (a) Geological map of the study area. The thick line is the ALCUDIA deep seismic reflection transect with the CDP numbers. (b) Generalized geological cross section along the grey line in the map, constructed from surface information. See auxiliary material for a larger version of this image.

phosphates and volcanic rocks [*Rodríguez-Alonso et al.*, 2004]. The geochemical studies of the Alcudian rocks support the existence of a Late Neoproterozoic active margin (Cadomian Orogeny) as a direct contributor to its sedimentary and magmatic contents [*Rodríguez-Alonso et al.*, 2004]. The Serie Negra, Malcocinado Formation and Alcudian succession are covered in some areas by Cambrian sandstones and limestones, or directly by Lower Ordovician quartzites. The stratigraphic relationships between the Serie Negra and the Alcudian succession remain unsolved. It has been argued that the Serie Negra could extend northwards of the Pedroches area under the Alcudian rocks [e.g., *Martínez Poyatos et al.*, 2001a], but a lateral change has also been proposed [e.g., *Vidal et al.*, 1994].

[14] The Ordovician to Devonian succession unconformably overlies the previous rocks. It is a 3000 m thick siliciclastic succession of alternating quartzitic and slaty formations deposited on a marine platform. The Lower Ordovician Armorican Quartzite Formation is a 500 m thick reference that leads topography and guides mapping.

[15] In the southernmost CIZ, remarkable Mississippian syn-orogenic sedimentation ('Culm' facies) took place in the Pedroches Basin, presently exposed around the Pedroches Batholith (Figure 2). This turbiditic formation is made up of monotonous alternations of dark slates and greywackes that, towards the bottom, also include conglomerates, mafic volcanics and minor limestones. The Culm thickness has been estimated to be at least 6000 m, implying important subsidence that has been explained in terms of D2 Mississippian extension coeval to the exhumation of the previously deep-seated rocks of the Central Unit [*Martínez Poyatos*, 2002]. Early Carboniferous magmatism took place coeval to sedimentation in the southern part of the Pedroches Basin (as well as in the OMZ and SPZ). Two relevant outcrops of Lower Carboniferous mafic rocks occur (Figure 2): (1) up to 2000 m of basaltic lavas in the southern limb of the Peraleda Anticline, and (2) a gabbroic pluton that conceals, along with Mississippian sediments and granites, the Central Unit towards the East.

2.4. Variscan Structures in the Southern Central Iberian Zone

[16] Early Variscan deformation was restricted to the Espiel Thrust Sheet located immediately to the north of the Central Unit (Figure 2), where Devonian D1 NE-vergent recumbent folds and associated ductile shearing have been described [*Martínez Poyatos*, 2002]. After erosion, the southern part of the Pedroches Basin (D2 Mississippian extensional event) unconformably covered the previous recumbent folds of the Espiel Thrust Sheet. Then, the Espiel Sheet was thrust to the NE (the Espiel Thrust; Figure 2) onto their relative Central Iberian para-authochthon during the starting of the D3 Pennsylvanian compression [*Martínez Poyatos et al.*, 1998].

[17] The most outstanding Variscan structures in the Schist-Greywacke Complex Domain are kilometer-scale upright to south vergent folds (Figure 2). They formed during the D3 Pennsylvanian event with associated slaty cleavage under very low-grade metamorphic conditions [*Martínez Poyatos et al.*, 2001b]. The folds usually trend WNW-SSE, from N120°E in the northwest to N090°E in the southeast. Locally, to the north of Almadén they rotate to a N-S direction as a result of a bending related to an inferred N130°E subvertical left-lateral shear zone [*Ortega Gironés*, 1986], or as a result of folds interference [*Julivert et al.*, 1983]. From south to north, the first-order folds are the Peraleda, Pedroches, Alcudia, Esteras, Navalpino and Valdelacasa anticlines, and the intervening Guadalmez, Almadén, Herrera del Duque, Guadarranque and Navalucillos synclines (Figure 2).

[18] Acid-intermediate plutonism and faulting took place during the late Variscan (D4 Pennsylvanian-Permian event) orogenic evolution. Granites are abundant in the CIZ, mainly in its northwestern sector. To the southeast, relevant batholiths are those of Pedroches and Mora (Figure 2), which display negative Bouguer gravity anomalies (Figure 4b). The Pedroches Batholith is made up of a main granodioritic pluton intruded by granitic bodies. The main faults strike NW-SE, parallel to the previous structures, and show left-lateral or normal displacements. In the studied area, the main faults are, from south to north: Azuaga, La Canaleja, Puente Génave-Castelo de Vide (PG-CV), and Toledo faults (Figure 2). The Azuaga Fault is a brittle, left-lateral strike-slip fault that bounds the Central Unit to the south, concealing the original thrust that superposed the Central Unit onto the OMZ. The Canaleja Fault is a brittle subvertical fault that down-threw the northern block [*Martínez Poyatos et al.*, 2001a]. The PG-CV Fault is a ductile to brittle, south dipping extensional shear zone [*Martín Parra et al.*, 2006]. The Toledo Fault [*Hernández Enrile*, 1991] has a low dip to the south and exhumed the Toledo Anatectic Complex, which is composed of granulite-facies (800°C, 5 kbar) pelitic migmatites and related granitoids with minor gabbros [*Barbero*, 1995].

3. Seismic Data Acquisition and Processing

[19] The ALCUDIA deep seismic reflection transect covers the area extending from the northern boundary of the OMZ to the Toledo Fault, thus spanning more than 200 km within the CIZ (Figure 2). The profile was recorded in 56 days (from May to July 2007) by an academic crew using a SERCEL 388, 400 channel device and five 22 Ton Vibroseis trucks (Table 1). To achieve a high resolution at shallow levels and to image dips as steep as possible (up to 80° near surface, but it decreases with depth), a long asymmetric spread with 35 m station spacing and 70 m Vibration Point (VP) interval was used. This configuration yielded a common midpoint (CDP) spacing of 17.5 m. The spread configuration maintained 120 active channels at the rear and a minimum of 120 at the front. This resulted in a variable nominal CDP fold, though always above 60, along the transect. Nonlinear sweeps in the 8–80 Hz frequency-range were generated by four Vibroseis trucks. Each VP consisted of six, 20 s long sweeps. Long sweeps were preferred to a greater number of sweeps in order to increase the source energy. The sweeps were diversely stacked in the field before correlation. Except for the station and VP spacing, the ALCUDIA profile was acquired with parameters (Table 1) that are typical of recent deep seismic reflection surveys: URSEIS [*Echtler et al.*, 1996], LITHOPROBE [*Cook et al.*, 1999], TRANSALP [*Gebrande et al.*, 2001], IBERSEIS [*Simancas et al.*, 2003].

Table 1. Acquisition Parameters

	Parameter
Source Information	
Source type	Vibroseis
Number of vibroseis trucks	4 (+1 spare) 22 TM
Number of sweeps × vibration point	6
Sweep length	20 s
Sweep type	Nonlinear
Sweep frequencies	8–80 Hz
Noise suppression	Diversity stack
VP interval	70 m
Total number of VP in transect	3622
Receiver Information	
Receiver station interval	35 m
Geofone array: number of geophones × station	12
Receiver type	10 Hz natural frequency
Total number of stations	7599
Recording time	40 s (20 after correlation)
Acquisition System Configuration	
Acquisition system	SERCEL 388
Number of active channels	240 minimum
Split spread	Asymmetric (120 active channels fixed at the tail)
Field filters	out
Nominal CMP	60

Table 2. Processing Flow

	Process	Parameter
	Data Preparation	
1	Field processing	SEGB-to-SEGY
2	Resampling	4 ms
3	Crooked-line geometry assignment	
4	Trace editing	
5	First break picking	
6	Elevation - static corrections	Floating datum 630 m
7	Refraction - static corrections	Generalized linear inversion
	Signal Enhancement	
8	Spherical spreading correction	
9	Notch filter	50 Hz
10	Time-variant bandpass filtering	Zero-phase: 19–75 Hz (0–1.3 s) 17–75 Hz (1.3–20 s)
11	Surface wave attenuation	F–K filter: 9 ms/trace
12	Air wave mute	
13	CMP sorting	
14	Velocity analysis	
15	Brute stack	
16	Surface-consistent residual static corrections	Stack-power maximization, maximum shift: 12 ms
17	F-k DMO in common offset gathers	Iterative velocity determination
18	Stack	
19	Coherency filtering	F–x deconvolution
20	Time migration	

[20] Coordinates x, y, and z were obtained using a high-precision differential GPS system. The seismic data were recorded in SEGB format and then transferred to DVDs in SEGY format with all of the geometry information, station and source location (station numbers and GMT coordinates, including topography). The overall population density along the surveyed area is relatively low, generating little noise and resulting in mostly high signal-to-noise ratio data. Therefore little trace editing and attenuation of cultural noise was required. The transect features an irregular, crooked line geometry. Certain shot locations needed to be skipped because of the existence of small villages along the survey. The gaps generated by these dwellings were fixed by an undershooting strategy, decreasing shot spacing at both sides of the village.

[21] The processing flow was designed to preserve relative true amplitudes (Table 2). Following the conventional processing, after trace editing (cultural noise, spikes, etc.), amplitude correction for spherical spreading was done followed by first break picking, elevation statics, refraction statics, trace balancing, velocity analysis, CDP sorting, staking, and migration. The raw data feature a relatively high signal-to-noise ratio (Figure 3). Most shots feature clear P-wave first arrivals characterized by high apparent velocities close to 5000 m/s. At shallow depths (up to 3 s two-way travel time, TWTT) (in this work all times are referred in TWTT), two prominent wave trains dominate the raw data: surface dispersive Rayleigh phases with apparent velocities within 3000 m/s and 1700 m/s, and a weak air-blast type of wave from the Vibroseis noise (Figure 3). The raw data feature frequencies between 10–50 Hz that clearly reflect the Vibroseis source. In an attempt to maximize the imaging capabilities of the recorded data, a conventional pre-stack signal enhancement processing flow was applied. It was designed specifically for high-velocity crystalline areas and followed considerations that were very effective for the processing of the IBERSEIS deep seismic reflection transect [*Schmelzbach et al.*, 2007]. Within the processing flow, special attention was devoted to trace editing, travel time picking of the first arrivals, and static corrections.

[22] The first key issue was the application of the crooked line geometry. Then, a spherical spreading correction g was applied. It consisted in:

$$g = At^{1.3} + x^{0.3} \quad (1)$$

where A is the amplitude, t the two-way travel time, and x is the offset between shot and receiver. The correction in (1) compensates for the amplitude decay due to increase in the radius of the wave front, i.e. the length of the ray path. Subsequently, surface-consistent zero-phase spiking deconvolution followed by time-variant band-pass filtering

Figure 3. Example of shot records (252, 272, 292, 312, 332, the vibrator point was located at stations 601, 641, 681, 719 and 757, respectively). Vertical axis is two way travel time (TWTT). (a) Raw shot gathers in which the direct P arrival (dP), the dispersive surface waves (Surface) and the Airy phases are indicated. (b) The same shot gathers after the application of signal enhancement processing steps (for more details in the processing sequence, see Table 2). The crust-mantle boundary is located at 10 s TWTT. (c) The power spectrum of the recorded signal, calculated by using shot gather, plotted up to Nyquist frequency of 125 Hz. See auxiliary material for a larger version of this image.

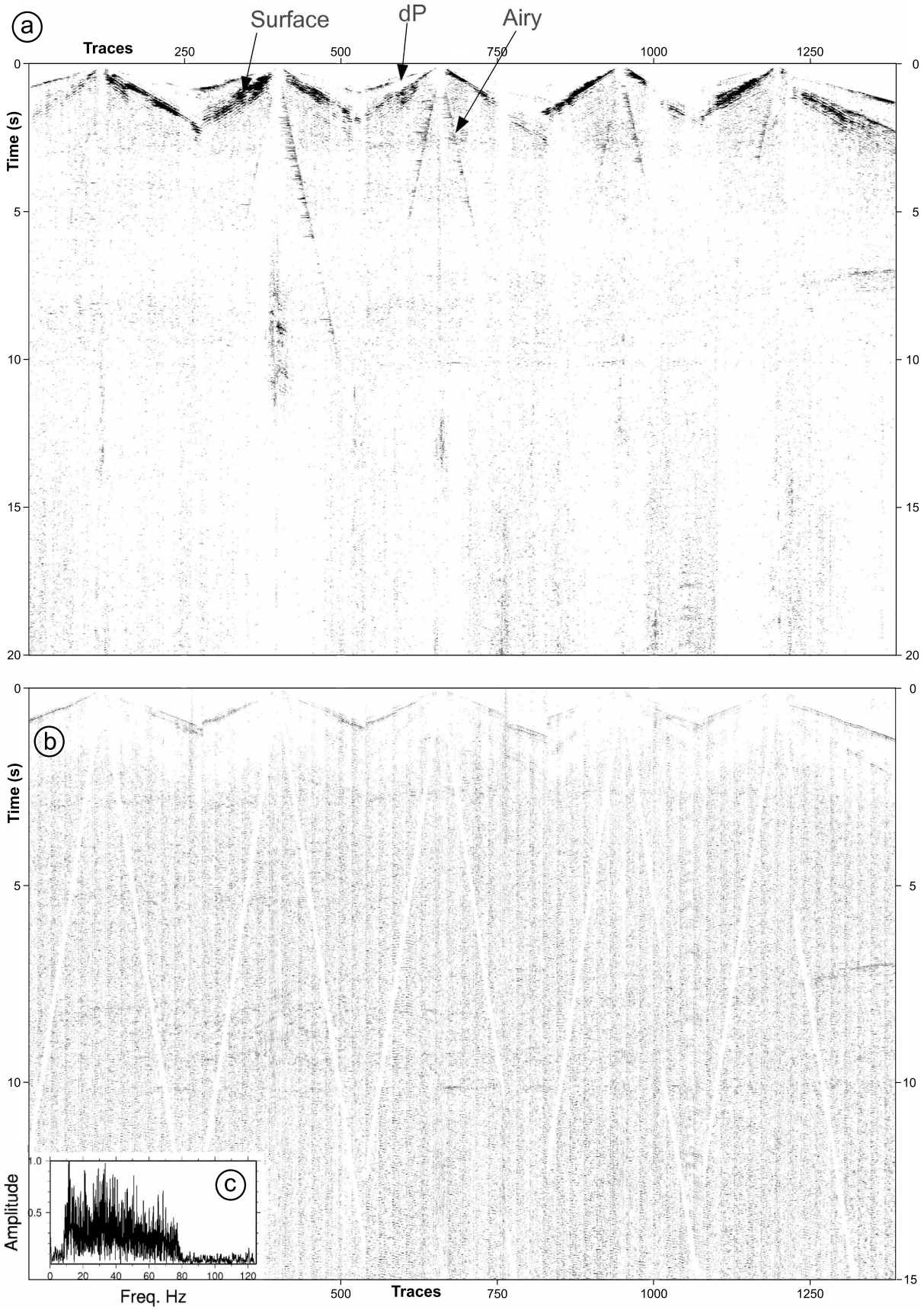
a
Surface
dP
Airy
Traces
250
500
750
1000
1250
Time (s)
0
5
10
15
20
b
Time (s)
c
Amplitude
1.0
0.5
0
20
40
60
80
100
120
Freq. Hz
500
Traces
750
1000
1250
15

Figure 3

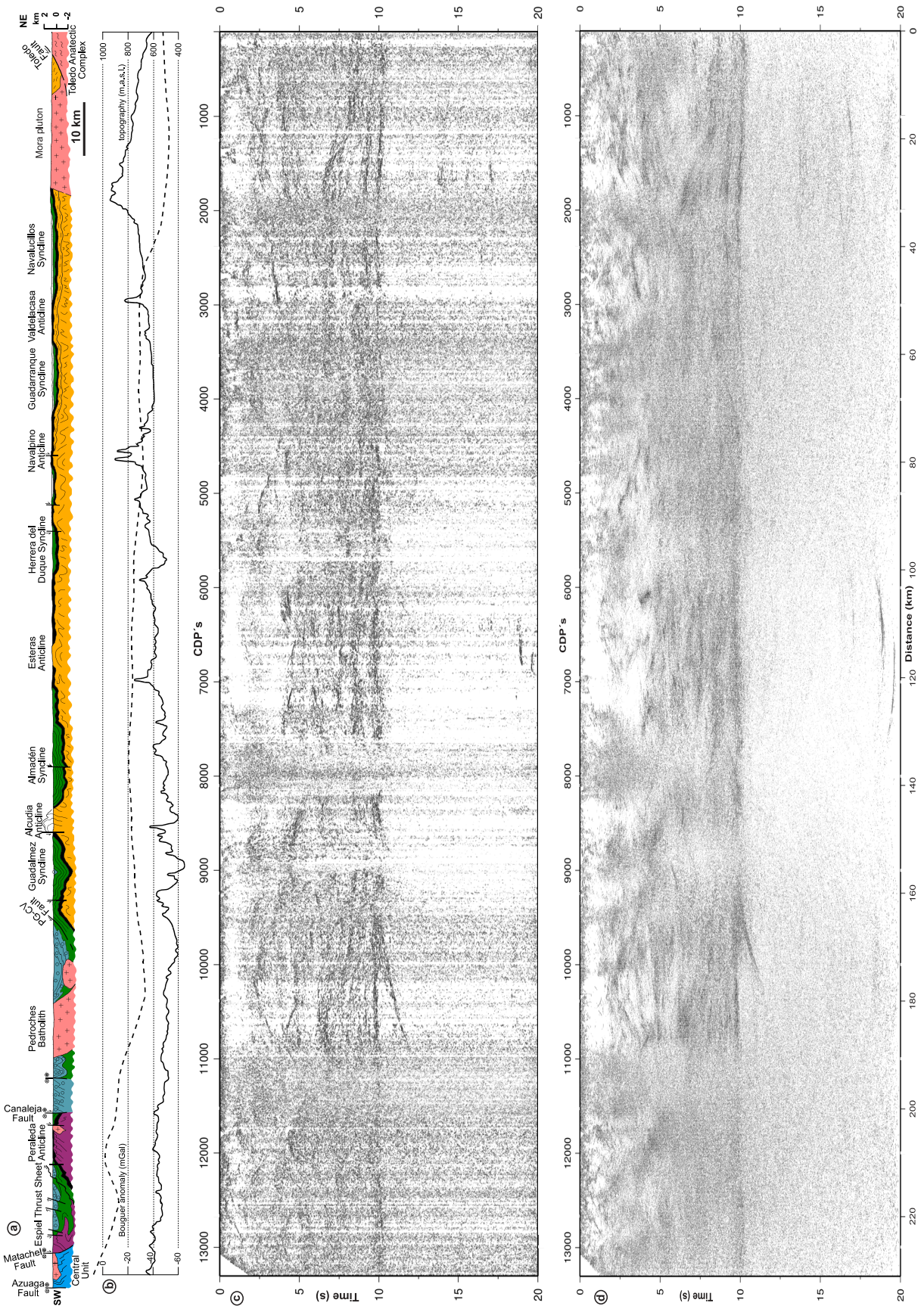
a
b
c
d
SW
NE
km
Azuaga Fault
Matachel Fault
Central Unit
Espiel Thrust Sheet
Peraleda Anticline
Canaleja Fault
Pedroches Batholith
PG-CV Fault
Guadalmez Syncline
Alcudia Anticline
Almadén Syncline
Esteras Anticline
Herrera del Duque Syncline
Navalpino Anticline
Guadarranque Syncline
Valdelacasa Anticline
Navalucillos Syncline
Mora pluton
Toledo Fault
Toledo Anatectic Complex
10 km
topography (m.a.s.l.)
Bouguer anomaly (mGal)
CDP's
Time (s)
Distance (km)

Figure 4

enhanced reflections at the expense of source-generated noise. The source wavelet corresponded to a frequency band of 8–80 Hz, i.e. the original input sweep frequency spectrum. The time variant band-pass filtering scheme consisted of a passband in the range of 22–45 Hz for the first 3 s, which was linearly shifted to a passband of 20–40 Hz for the data window from 4 to 7 s, and finally to a passband of 10–35 Hz for the latest data window between 8 and 12 s. An effort was also dedicated to attenuate the surface waves by frequency-wavenumber filtering (F-K) the first 5 s time windows of the recorded shot gathers. The attenuation of the surface wave energy was more relevant to processing than the static corrections, probably due to the relatively thin and anomalously fast weathering layer. A top mute function reduced some of the remaining source-generated noise. In order to decrease the effects of the source- and receiver-coupling differences, a surface-consistent amplitude balancing function was applied. Two passes of velocity analysis were performed: a conventional semblance velocity analysis provided the first estimation of the stacking velocity model. This model was later improved by constant velocity stacks in specific areas. Finally, a surface consistent residual static correction that removed the remaining event misalignments in the normal moveout (NMO) corrected CDP gathers, was applied. To resolve the conflicting dips of the shallow events, a dip moveout (DMO) processing step was included. DMO corrections were estimated in an iterative procedure [*Yilmaz*, 2001]. Then NMO and DMO were applied and another pass of velocity analysis was carried out. A 50% stretch mute was applied to the CDPs before stacking. After stacking, the data were projected onto a straight line for migration. F-X deconvolution was applied to the stacked data prior to time migration in order to decrease incoherent noise and increase the lateral coherence of the reflections. A post-stack time migration step was then applied using a smooth velocity field about 5–10% slower than the root mean square (rms) stacking velocities (Table 2). Several runs were carried out with different algorithms and different velocity fields; finite differences and Stolt approaches provided similar results. For plotting purposes, the stack and the time migrated data sets were coherently filtered.

4. The ALCUDIA Seismic Reflection Image

4.1. General Considerations

[23] The ALCUDIA deep seismic reflection image (Figure 4) reveals an internal architecture of the crust more complex than expected from surface structures. The upper crust, characterized in most of the profile by upright folds, covers the interval 0–4 s (∼0–11 km depth) (in this work depth equivalents have been estimated from the seismic wave velocities modeled for the southernmost CIZ [*Palomeras et al.*, 2009]). Its seismic image reveals weakly reflective areas as compared to the high amplitude reflectivity characteristic of the lower levels of the crust. A few vertical stripes of about 10 km width reveal zones of low signal-to-noise ratio. The mid-lower crust goes from approximately 4–5 s (∼11–14 km depth) down to 10 s (∼30 km depth). It features high amplitude arcuated events along most of the profile. The crust is highly laminated below 5–6 s (∼14–17 km depth) and exhibits evidences of outstanding structures affecting the lamination (Figure 5). The Moho discontinuity is identified as a high-amplitude band of reflectivity located at approximately 10 s (∼30 km depth). It is placed at a sharp break in reflectivity on top of the low reflective upper mantle. In the southern part of the image, just below 10 s, a prominent high-amplitude south-dipping feature suggests an imbrication involving the mantle (Figure 5). Deeper seismic reflectors in the lithospheric mantle are very scarce and short, the most outstanding appearing at CDP 7000 and 19 s (Figure 4).

[24] The profile can be divided into three, approximately equal segments (4500 CDPs or 80 km long each), based on its reflectivity and geological interpretation: northern, central and southern segments. The central segment is the simplest. North and south of it, the pattern of reflectivity is more complex, thus providing evidence for more complicated relationships between the upper and lower crust. Accordingly, we will start the interpretation of the profile in the central segment, describing later the northern and southern segments.

4.2. Central Segment

[25] The central segment corresponds to the interval from CDPs 4000 to 9000 (Figures 4 and 5). From a geological point of view, it covers the area from the Guadarranque Syncline to the Guadalmez Syncline (Figure 2). The most outstanding feature is the reflectivity contrast between a nearly transparent upper crust and a very reflective middle-lower crust.

[26] The seismic image of the upright folds described earlier appears in places as small discrete synclines or opposing dips (e.g., at CDPs 4000, 5600, 8000, or 9000) that reach depths of 1 s (∼2.5 km depth) (Figures 4 and 5). A number of north-dipping reflectors (CDPs 4500 to 5500, 2–3 s) project at surface at around CDP 6600 near the Esteras Anticline (Figure 4), being tentatively interpreted as thrusts related to this anticlinal structure (Figure 5d). They do not appear to reach the surface and seem to sole down at mid crustal levels in a detachment placed at approximately 4–5 s (∼11–14 km depth), on top of the highly reflective (lower-middle) part of the crust. Additionally, arcuated bands of low amplitude reflectivity at approximately 2 s and between CDPs 5000 to 7500 may correlate with the km wavelength folds mapped at surface (Figures 4 and 5).

[27] From 4–5 s down to the Moho, the crust shows a very reflective character. We will refer to this part of the crust as middle-lower crust. The subhorizontal reflectors are only slightly braided in places (e.g., CDP 6200, 7 s; Figures 4

Figure 4. ALCUDIA deep seismic reflection profile with relevant geological and gravimetric constraints. (a) Geological cross section along the seismic transect with key geological features labeled with the local toponyms. (b) Topography and Bouguer gravity anomaly profiles along the transect. (c) Coherency filtered stacked image of the ALCUDIA deep seismic reflection transect. (d) Time migration image of the stack displayed in Figure 4c. In Figures 4c and 4d the horizontal axis corresponds to CDP numbers and the vertical axis corresponds to two way travel time (TWTT). See auxiliary material for a larger version of this image.

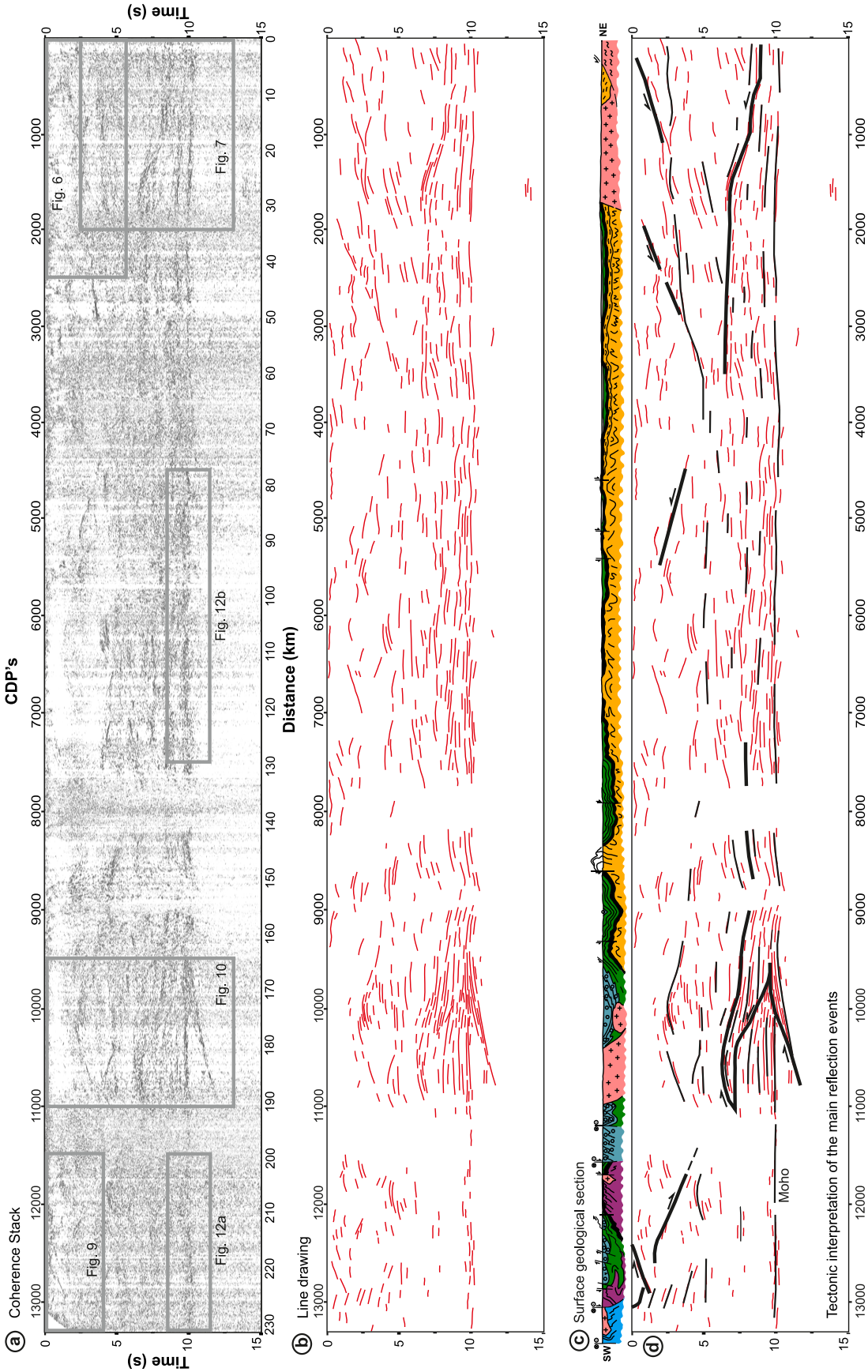

Figure 5. Interpretation of the seismic image. (a) Coherency filtered stacked image of the ALCUDIA deep seismic reflection transect with location of the windows zoomed in Figures 6, 7, 9, 10, and 12. (b) Line drawing of the most conspicuous reflectivity (in light red) derived from the stack shown in (a). (c) Surface geological cross section along the seismic transect. (d) Large-scale interpretation of the line drawing. The reflection fabrics and the relatively-high amplitude and laterally coherent events (highlighted as thin black lines) suggest a large-scale structure (bold black lines). See auxiliary material for a larger version of this image.

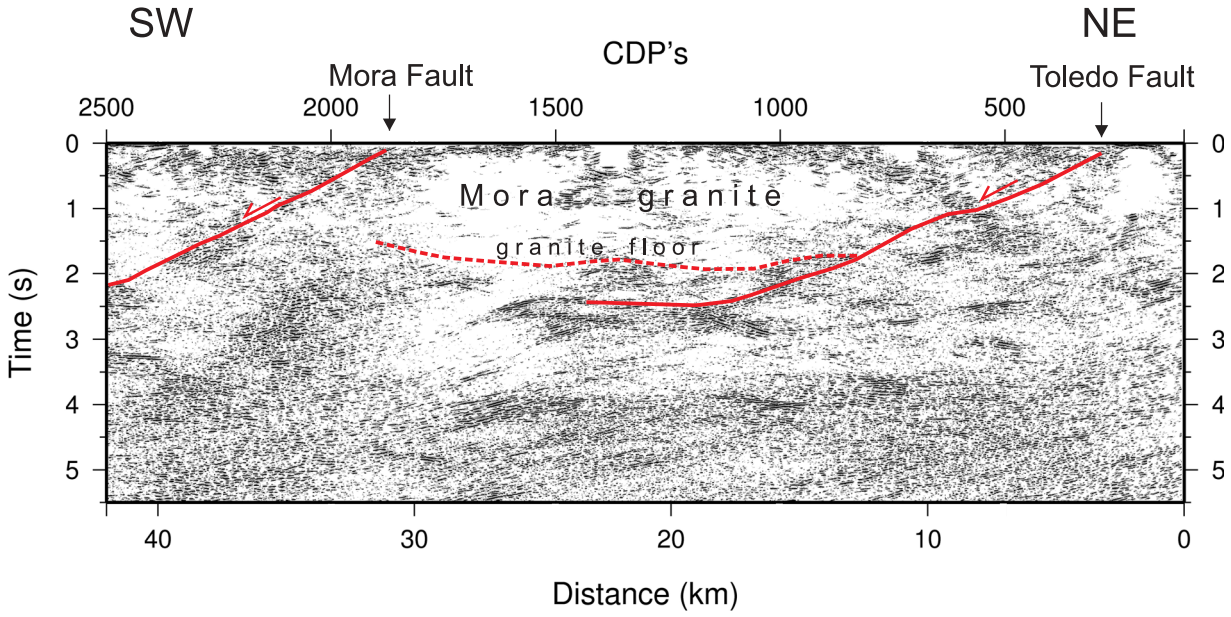

Figure 6. Detailed image (time migrated) of key geological structures within the shallow crust in the northern sector of the ALCUDIA deep seismic transect. Interpretation in red (see text for further explanation). The Mora granite is imaged as a transparent zone. See auxiliary material for a larger version of this image.

and 5). The interpretation of these dense reflectors is controversial and will be addressed in the discussion.

[28] The seismic image of this central segment of the ALCUDIA profile raises the question of how is shortening accumulated in the upper-crustal folds (geological cross section, Figure 2) accommodated in the lower crust. A key to answer this question resides in the northern and southern segments of the profile.

4.3. Northern Segment

[29] This segment goes from CDPs 100 to 4000 (Figures 4 and 5, with selected windows in Figures 6 and 7). From a geological point of view, it goes from the Toledo Anatectic Complex to the Guadarranque Syncline (Figure 2). As in the central segment, the crust can be divided into a less reflective upper part and a very reflective mid-lower part.

[30] The reflectivity of the upper crust in the northern segment is more intense than in the central segment. Thus, the upper crust here is characterized by reflectors that correlate with geological structures identified at surface (Figure 6). First, a south-dipping reflective band projects to the surface at approximately CDP 200, in coincidence with the Toledo Fault (TF). The TF south-dipping reflectivity soles down at 2.5 s (~6.5 km depth) into a high-amplitude, wavy sub-horizontal prominent reflector interpreted as a detachment. Second, from CDP 1900 and 1 s, another group of south-dipping reflectors soles down to around CDP 2900 and 3 s within the same inferred detachment (Figure 5). This second south-dipping reflector is also interpreted as a normal fault (the Mora Fault, MF) which truncates low-dipping reflectors at both sides (Figure 5) and projects at surface in the southern boundary of the Mora granite. TF and MF define a system of synthetic faults; in-between, the Mora granite appears as a transparent body with a well-defined floor at 2 s (~5 km depth) (Figure 6). The prominent reflector where TF and MF sole down dips gently to the south, descending from 3 s at CDP 2500 to 5 s at CDP 3500 (Figure 5). This descent, which we interpret as the hanging wall ramp of an underlying thrust previous to TF and MF, is a key feature for the tectonic interpretation of this northern segment.

[31] The lower-middle crust shows high-amplitude and laterally coherent parallel reflections (Figure 7). A prominent reflector rises from 8 s at CDP 1000 to 6.5 s at CDP 2000, defining a flat-ramp-flat surface. Beneath it, a high amplitude horizontal reflection fabric is truncated by the ramp. Above it, the reflection fabric is horizontal between CDPs 100 and 1200 at 7 s, and south dipping above the ramp (CDPs 1000 to 2000 at 5–6 s). These geometrical relationships suggest a flat-ramp-flat thrust surface with truncations in the footwall and bending accommodation in the hanging wall (Figures 4, 5, and 7). The geometry of this structure is completed with the already mentioned hanging wall ramp. The identification of both, hanging wall ramp and footwall ramp, constrains the thrust displacement to ~35 km (Figure 8). Two models are presented to explain this structure: in one, the lower crustal thrust roots in the Moho (Figure 8a); in the other, the thrust penetrates into the mantle (Figure 8b). Both models involve crustal thickening and a culmination, before normal faulting (D4), marked by the inferred position of the Lower Ordovician Quartzite (broken red line in Figure 8). The TF separates the high-grade metamorphic domain of the Toledo Anatectic Complex from a low-grade region to the south (Figure 2) [*Hernández Enrile*, 1991]. According to *Barbero* [1995], peak metamorphic conditions in the anatectic domain were around 800°C and 4–6 kbar, whereas to the south the metamorphic conditions did not exceed 400°C (no biotite in pelites) and 2 kbar (estimated emplacement pressure for the Mora pluton) [*Andonaegui*, 1990]. Accordingly, the pressure gap

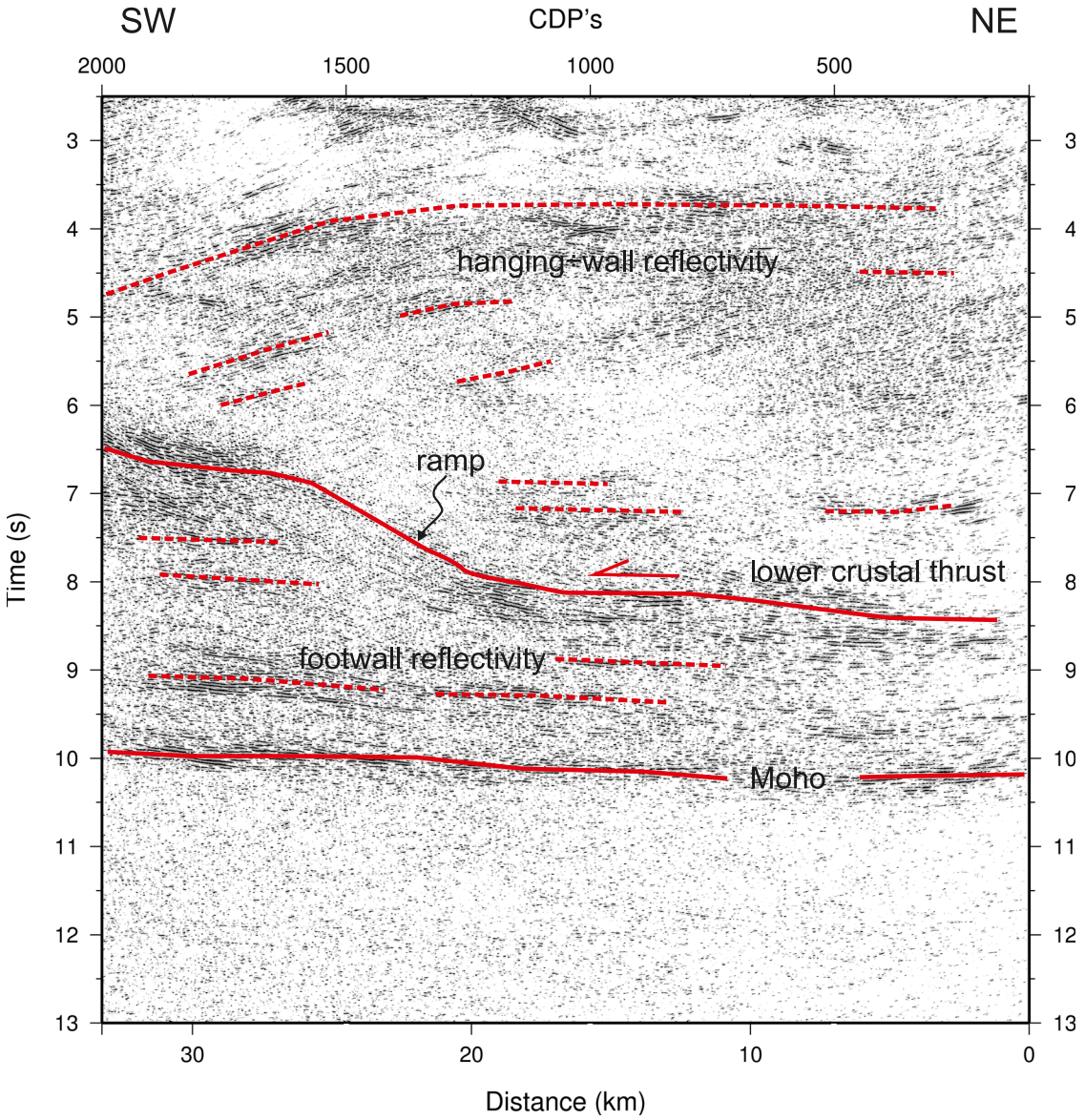

Figure 7. Detail of the crustal section (time migrated) of the northern sector of the ALCUDIA deep seismic reflection transect, displaying the mid-lower crust and Moho. Interpretation in red (see text for further explanation). See auxiliary material for a larger version of this image.

produced by the TF is ~3 kbar. The two models depicted in Figure 8 may account for this pressure gap.

4.4. Southern Segment

[32] This segment spans from CDPs 9000 to 13450 (Figures 4 and 5 and selected windows in Figures 9 and 10). From a geological point of view, it goes from the Guadalmez Syncline to the Central Unit (i.e., the OMZ/CIZ suture, Figure 2). The mid-lower crust is again more reflective than the upper crust, though the latter is more reflective than in the rest of the profile and shows interesting features related to the upper crust structure.

[33] The upper crust has north and south dipping reflectors down to 4.5 s (~12 km depth). They represent the upright folds and faults that characterize this sector (Figure 2). At CDP 9000 and above 1 s (~2.5 km depth), there are reflections defining the Guadalmez Syncline (Figures 2 and 5). Towards the southern end of the profile, there are reflections above 2 s (~5 km depth) associated with the Peraleda Anticline (at CDP 11800) and the Espiel Thrust (which projects to the surface at CDP 12300) (Figures 2 and 9). Between CDPs 9700–10800 and 2–3 s (~5–8 km depth), continuous reflectors delineate another antiform (Figures 5 and 10). These structures are part of a continuous fold train apparently detached at 4.5 s from the underlying reflective mid-lower crust.

[34] A different geological meaning is attributed to a north-dipping reflector that reaches 4 s (~11 km depth) at CDP 11800 and projects to surface at CDP 13100 (Figure 5). It is interpreted as the Matachel normal fault located at the top of the Central Unit (Figures 2 and 9), which was also imaged by the IBERSEIS seismic section (Figure 1) [*Simancas et al.*, 2003]. At CDP 12300 and 2 s, this fault truncates the underlying low-dipping reflectivity of the

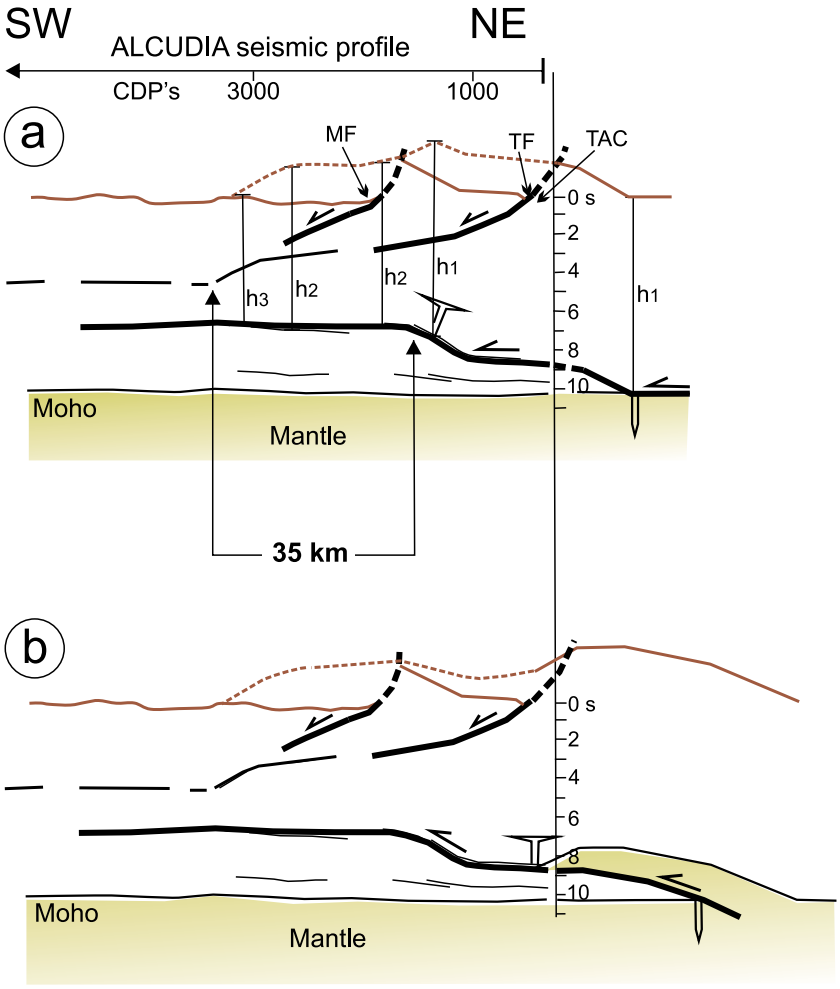

Figure 8. Two tectonic models of the northern sector of the ALCUDIA transect, resulting from the structures interpreted in Figures 6 (upper crust normal faults) and 7 (lower crustal thrust). (a) The lower crustal thrust roots at Moho level. (b) A wedge of mantle material is also involved in the thrust. TF: Toledo Fault; MF: Mora Fault; TAC: Toledo Anatectic Complex; h1: reference crust thickness; h2 and h3: successive thicknesses of the collapsing hanging wall of the thrust. See auxiliary material for a larger version of this image.

Central Unit (Figure 9). Finally, at CDP 12800 and 1 s, the Matachel Fault appears to be offset by the Espiel Thrust (Figure 9). This offset supports the geological evidence that D2 Mississippian extension (Matachel Fault) pre-dates the D3 Late Carboniferous compression (Espiel Thrust and upright folds) [*Martínez Poyatos et al.*, 1998].

[35] Within the mid-lower crust, the reflectivity is intense from 4.5 to 10 s (~12 to 30 km depth) (Figures 5 and 10). After a horizontal trajectory at 7 s from CDPs 11000 to 10500, a reflector dips to the north to reach the Moho at CDP 9600. Above this north-dipping reflector, the reflectivity depicts an antiformal wedge tapering to the south; below it, the lower crust shows subhorizontal reflectors truncated by the north-dipping reflector. Finally, a mantle wedge is imaged between CDPs 9500–10800 and 10–12 s (~30–37 km depth). This wedge is defined by a conspicuous reflection zone dipping to the south and thinning (from 1 to 0 s) in the same direction. This reflection zone is overlaid by a non-reflective area (Figures 4, 5, and 10). To sum up, two reflections with opposite dip converge at the Moho, depicting a crocodile-type and composite crust-mantle wedge, which impinges into the adjacent lower crust (Figure 10). The geometry of this wedge structure accounts for ~30 km shortening in the lower crust. Above it, in the upper crust, the Mississippian Pedroches Basin was inverted by D3 Late Carboniferous folding, which we relate to the wedging in the lower crust (Figures 11a and 11b). Laterally to the NW, this wedge correlates with the crocodile-shaped structure identified in the northern end of the IBERSEIS seismic profile (Figures 1 and 11c) [*Simancas et al.*, 2003].

5. Discussion

5.1. Reflective Lower Crust

[36] Traditionally, the densely reflective bottom of the crust has been interpreted as the petrological lower crust of mafic and felsic granulites [e.g., *Griffin and O'Reilly*, 1987]. In the ALCUDIA seismic profile, the interpretation of the lower-crust reflectors in terms of compositional layering and/or lamination is uncertain. Some geophysical data

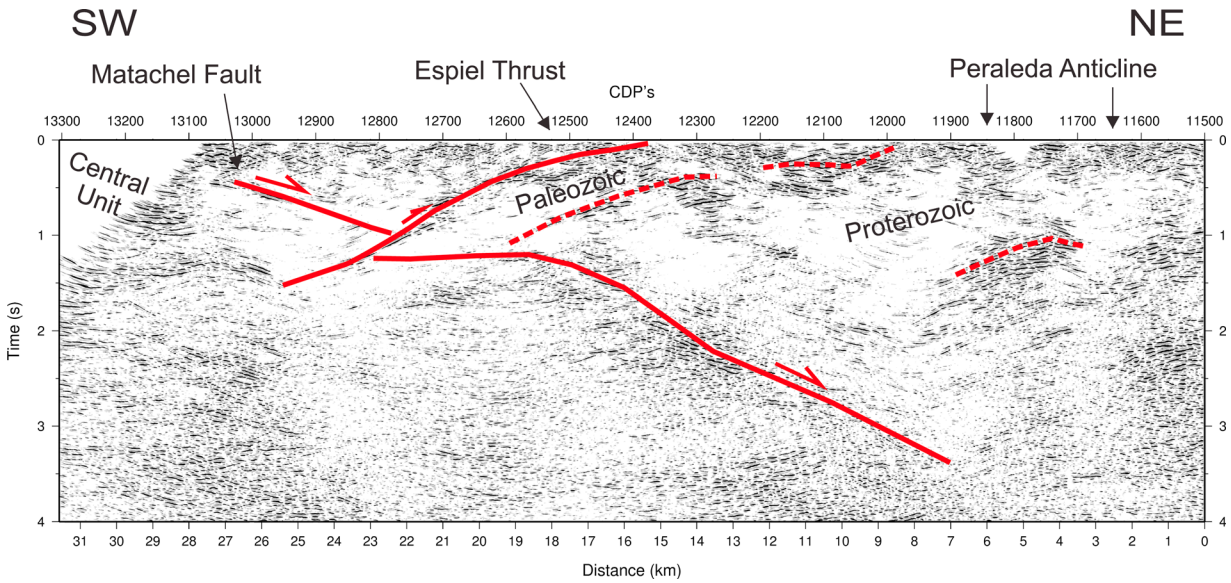

Figure 9. Seismic time migrated image of the shallow crust in the southern end of the ALCUDIA deep seismic transect. This figure images the suture (Central Unit) between the Ossa-Morena Zone and the Central Iberian Zone. Interpretation in red (the continuous lines denote faults, while discontinuous lines indicate lithological limits). See auxiliary material for a larger version of this image.

suggest a seismically fast and electrically conductive material, probably mafic in composition, in the middle-lower crust of the southern CIZ. In this respect, dense wide-angle seismic data, partly superposed to the IBERSEIS profile, show relatively high seismic velocities from 14 to 32 km depth, thus providing evidence for a prevailing mafic composition [*Palomeras et al.*, 2009], most probably interbedded rocks with contrasting seismic properties, but with average velocities and densities of mafic rocks [*Palomeras et al.*, 2011]. A magnetotelluric transect coincident with the ALCUDIA profile has revealed a persistent conductive body in the mid-lower crust all along the transect [*Pous et al.*, 2011], which is compatible with the above interpretation. However, it is not straightforward that the highly reflective zones represent the petrological lower crust. Its thickness, up to 6 s in some places (>18 km), would imply the existence of a thick layer of dense granulites that would have a conspicuous gravity anomaly, which has not been detected. Thus, the lower crust could be an imbrication of felsic to intermediate granitoids interlayered with mafic and ultramafic rocks [*Smithson*, 1989].

[37] Extensional episodes triggering felsic and mafic magmatic activity, as well as pervasive ductile shearing, have also been suggested as contributors to the reflectivity in the lower crust [*Allmendinger et al.*, 1987; *McCarthy and Thompson*, 1988; *Mooney and Meissner*, 1992; *Meissner*, 1999]. The CIZ crust studied by the ALCUDIA profile has not been affected importantly by extensional tectonics that might allowed massive intrusion of igneous material at deep crustal levels, at least during the Paleozoic (Variscan) evolution or later. For the same reason, we cannot give particular support to the possible development of extensional pervasive ductile shearing that might have affected the lower crust. However, D2 Mississippian extension, that extensively affected the SPZ, the OMZ and the southernmost CIZ, might have partly heated the CIZ and contributed to the onset of ductile deformation in the lower crust during D3 Pennsylvanian compression. On this regard, one of the best constraints on the origin of the high reflectivity of the lower crust refers to its age. Obviously, the lower crust was affected (folded and truncated by thrusts) by the D3 Pennsylvanian compression in the northern and southern segments of the profile, and maybe locally by the D4 late orogenic extension. Therefore, we can state that reflectors are coeval or older than the thrust and wedge deformation affecting the lower crust, i.e. lamination must be Late Carboniferous or older.

[38] The seismic structure observed in the ALCUDIA section, largely reminds that of the suprastructure-infrastructure model as revisited by *Culshaw et al.* [2006]. This model explains the existence of a seismically transparent upper crust detached from a laminated and very reflective lower crust as result of the deformation of a relatively hot crust due to shortening provoked by an indentor. According to this model, the transparent upper crust in the ALCUDIA section would represent the first stages of D3 compression, while the reflective mid-lower crust would record ductile deformation after D1 thickening and D2 heating. Finally, the separation of upper and mid-lower crust is a high strain zone imaged as a detachment. Consequently, the mid-lower crust lamination would be syn-orogenic and might be affected by ongoing D3 Pennsylvanian compression. On the other hand, we cannot rule out the possibility that the high reflectivity was produced by an earlier Variscan episode, in particular the extensional and magmatic D2 Mississippian episode. However, the D2 event is well developed in the southern part of ALCUDIA and to the south of it (in the IBERSEIS transect), but weakens northward in the CIZ (Figure 11a), while the reflective lower crust persists. Besides, the lower crust lamination might have also developed during an older event, perhaps the Late Proterozoic Cadomian evolution [e.g., *Rodríguez-Alonso et al.*, 2004].

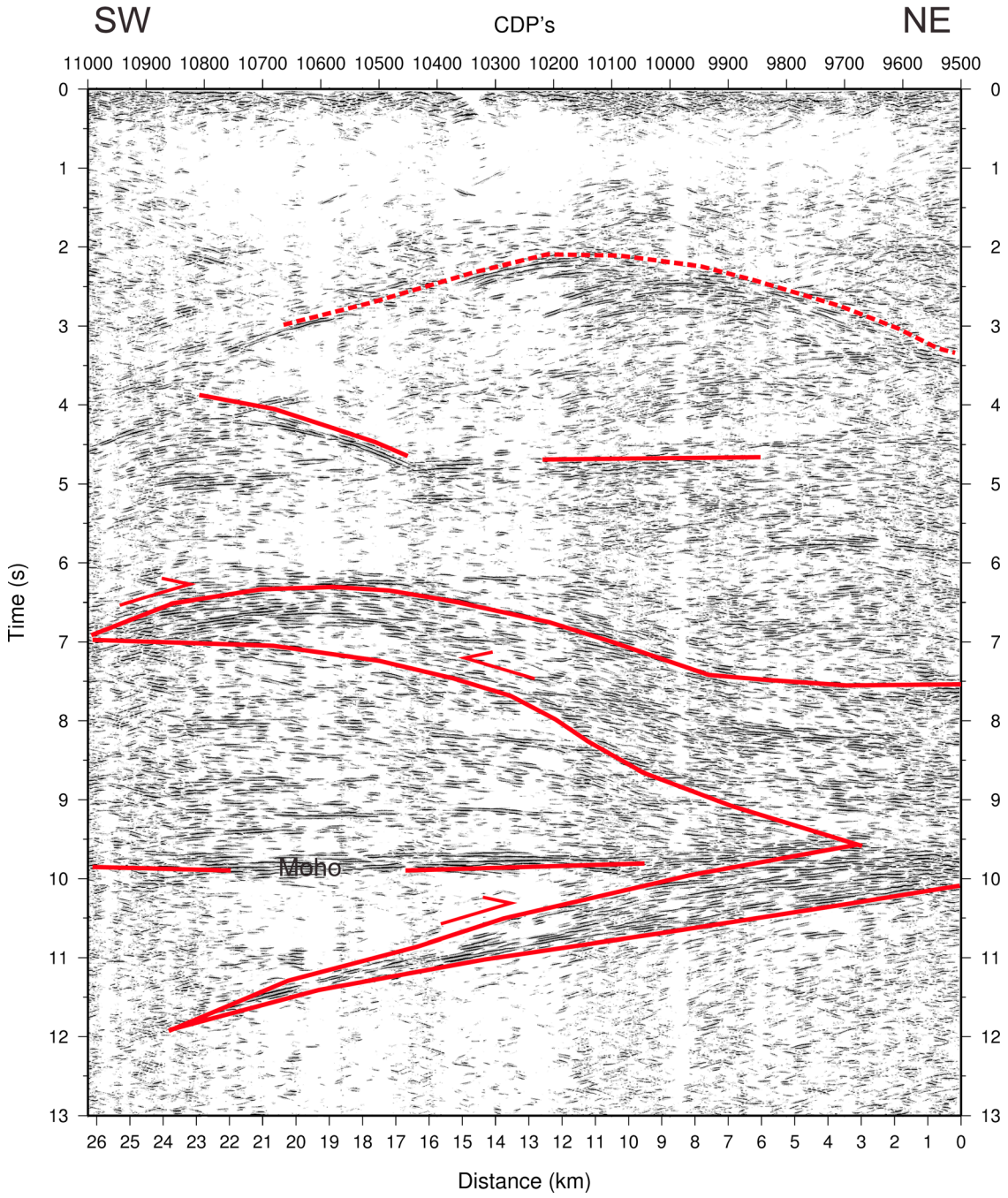

Figure 10. Window of the ALCUDIA seismic stacked image beneath the Pedroches Basin, revealing a tectonic wedge in the lower crust that also involves the mantle. Antiformal structures (arched reflectivity fabrics) appear in the upper crust, beneath the Pedroches Mississippian Basin. See auxiliary material for a larger version of this image.

[39] Seismic profiles shot across other hinterland Variscan zones of the Iberian Peninsula show also a very reflective thick laminated lower crust, which seems to be affected by Variscan compression (e.g., ESCIN-3.3 [*Ayarza et al.*, 1998]). On the view of the new suprastructure-infrastructure concept, the lamination observed in that seismic profile, and even in others across the European Variscides, might also be interpreted in accordance to this model, also used for the Western Superior Province of Canada [*Culshaw et al.*, 2006].

5.2. Moho Discontinuity

[40] One of the most relevant and geologically important boundaries on the ALCUDIA deep seismic transect is the crust-mantle transition. The base of the crust is defined as the sharp transition from a relatively high-amplitude reflectivity fabric to an almost transparent zone below, which is classically interpreted as the upper mantle. This is a dominant feature of high-quality deep seismic reflection profiles [e.g., *Klemperer et al.*, 1986; *Hammer and Clowes*, 1997].

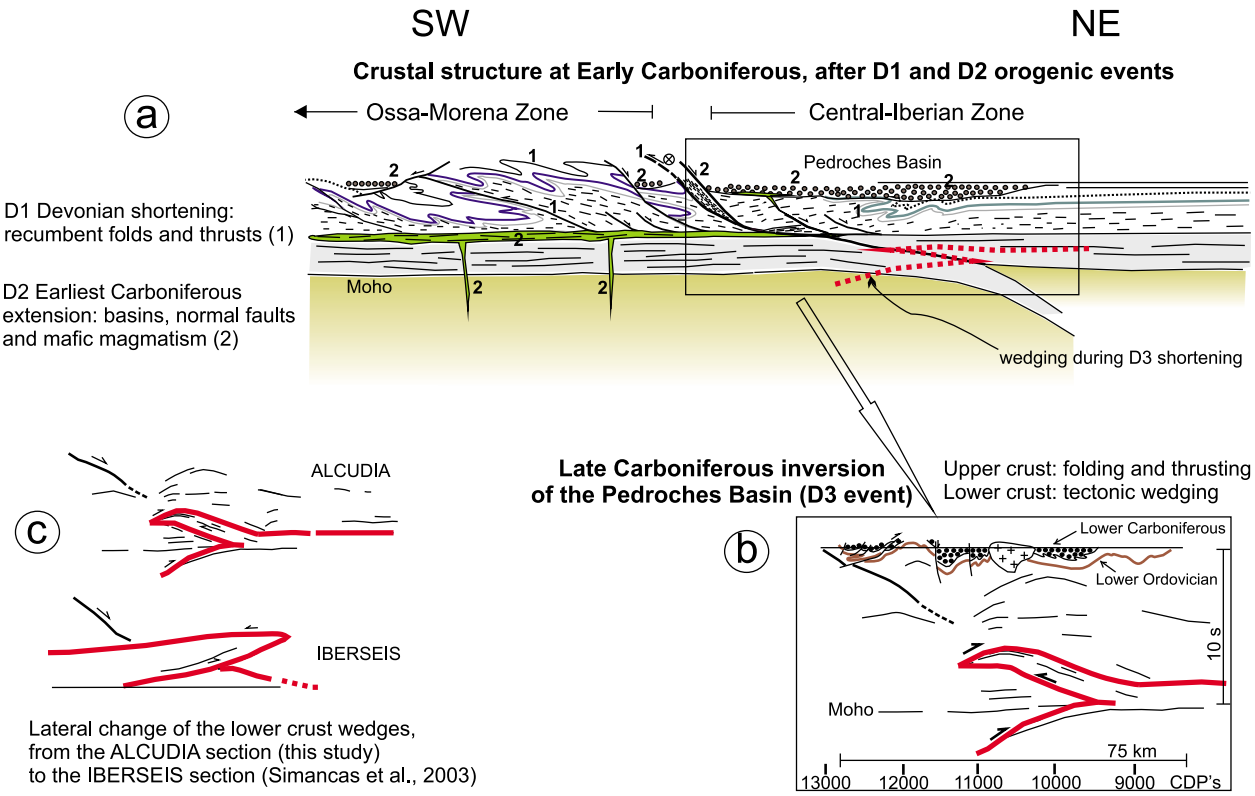

Figure 11. Tectonic model for the interpreted structures in the southern segment of the ALCUDIA seismic transect (Figures 9 and 10). (a) Sketch, not to scale, of the crustal structure after D1 (Devonian compression) and D2 (Mississippian extension) orogenic episodes. (b) Sketch, drawn to scale, of the crustal structure after D3 orogenic episode (Pennsylvanian compression). (c) Comparative views of equivalent portions of the ALCUDIA and IBERSEIS [*Simancas et al.*, 2003] deep seismic reflection transects (Figure 1), showing a lateral change of lower crust tectonic wedges with opposite vergences. See auxiliary material for a larger version of this image.

The reflection signature at the base of the crust, its overall geometry and its internal fabric have led to a series of different interpretations for the crust-mantle boundary [e.g., *Hynes and Snyder*, 1995; *Hammer and Clowes*, 1997; *Carbonell et al.*, 1998, 2002; *Cook*, 2002]. On the ALCUDIA profile, the relatively high-amplitude reflection or group of reflections located at approximately 10.2 s (~30 km depth) (Figure 4) are interpreted as the crust-mantle boundary. The geometry of the Moho is remarkably horizontal, although not totally flat. The ALCUDIA section (Figure 4) extends the Moho mapped by the normal incidence IBERSEIS [*Simancas et al.*, 2003] and the wide-angle [*Palomeras et al.*, 2009] surveys more than 200 km to the northeast.

[41] In detail, the crust-mantle transition in the ALCUDIA transect features local differences in the seismic signature. These are displayed in the seismic fabrics from the lower crust down to the upper mantle (Figures 4 and 12). The most outstanding feature is the south-dipping high-amplitude band of reflectivity located beneath CDP 10000, which dips into the mantle with a lateral extension of approximately 25 km (the lower lip of a "crocodile" structure). This structure probably represents the boundary between the OMZ and the CIZ at depth. The imaged Moho shows small differences between these two zones (Figure 12). The band of reflections interpreted as the Moho beneath the CIZ features higher amplitudes than those of the OMZ to the south of the dipping structure at CDP 10000. Differences in geometry between the OMZ Moho and the CIZ Moho can also be identified (Figure 4). The OMZ Moho is characterized by very flat, horizontal reflectors, while the CIZ one is characterized by limited undulations (Figure 4). In detail (Figure 12b) the undulations in Figure 4 are a result of patches of reflectivity beneath 10.0 s (beneath the Moho) that are more prominent to the north (e.g., centered at CDPs 5500 and 4800). Farther to the north (between CDPs 100–3500) the base of the crust is characterized by two prominent high amplitude reflectors, which appear to be slightly folded and almost parallel to each other (Figure 4).

[42] The differences in the crust-mantle signature between the OMZ and the CIZ may reflect local differences in the tectonic processes affecting them. One possibility considers that this boundary responded differently to deformation in both zones. The Moho undulations could have accommodated a small amount of shortening during compression. In contrast, the sharp horizontal Moho beneath the OMZ could represent horizontal shear zones, indicating a higher degree of decoupling between the OMZ crust and the mantle beneath. However, the OMZ Moho might also indicate the influence of D2 Mississipian extension, which affected the whole OMZ and barely the CIZ. The 60 km long almost parallel two reflection events imaged in the northern segment of the transect (from CDPs 100 to 3500, one event

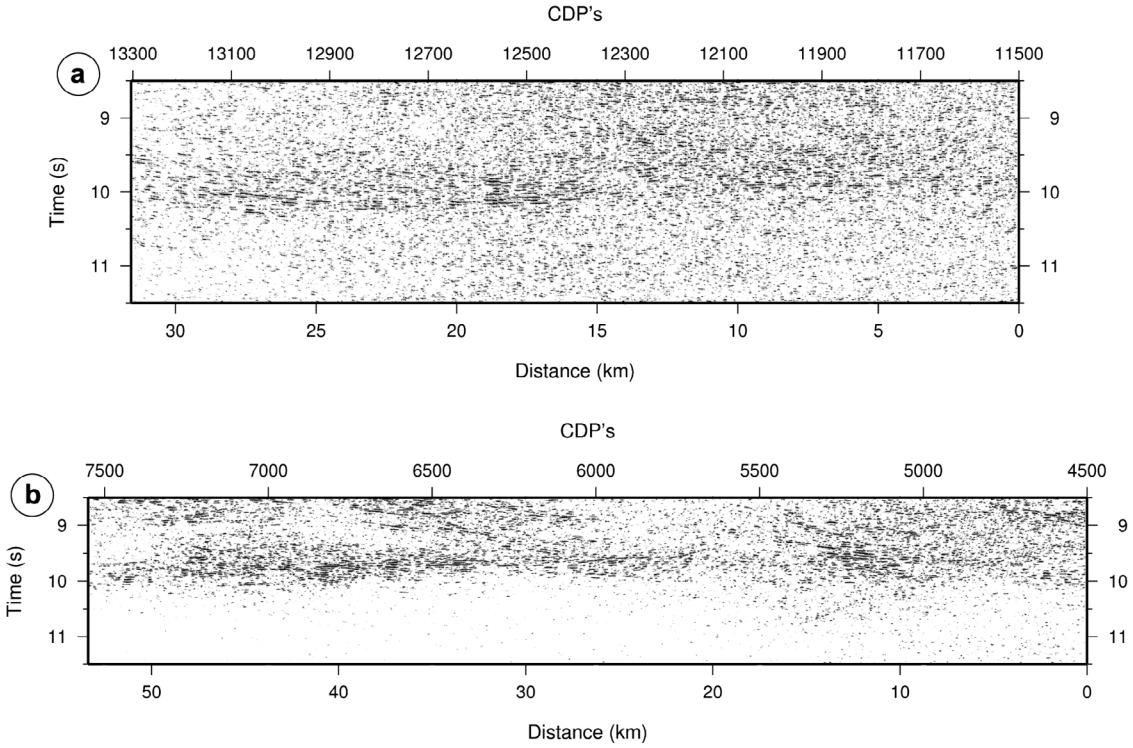

Figure 12. Two detailed (time migrated) images of the Moho discontinuity in the ALCUDIA deep seismic reflection transect. (a) The crust-mantle transition zone beneath the Ossa Morena Zone (southern part of the profile): a relative high-amplitude reflection band that defines the Moho discontinuity reveals relatively sharp horizontal aligned reflection segments. (b) The crust-mantle transition zone beneath the Central Iberian Zone (central part of the profile): the Moho discontinuity features average-amplitude reflections that reveal dipping structural features that enter the mantle, suggesting an undulating boundary. See auxiliary material for a larger version of this image.

located at 10 s and the other one at 9 s; Figure 4) could be interpreted as two shear zones, suggesting a duplex structure at the crust-mantle boundary and within the lower crust. Nevertheless, other interpretations such as two deformed sill intrusions cannot be ruled out.

[43] The steady long-wavelength decrease of the Bouguer gravity anomaly towards the north (Figure 4) suggests that either a change in rock density or in crustal thickness must exist. The reflective mid-lower crust seems to thin northward on the profile and accordingly might play a role in gravity signature. On the other side, crustal thickness does not seem to change significantly. However, accurate time-migration should be carried out in order to assess whether or not the lithologies and structure of the upper crust influence the position of the seismic crust-mantle boundary. Furthermore, at the northern end of the profile, the thinner reflective mid-lower crust might also imply a change in velocities that should affect the imaged depth of the seismic Moho. Gravity modeling and a better knowledge of the crustal velocities based on high-resolution wide-angle data should be carried out in order to answer this question.

[44] The sharp Moho (about 0.5 s) at an almost constant depth (Figures 4, 5, and 12) does not accord with the orogenic scenario envisioned for Carboniferous time. Most of the lower crust reflectors are sub-parallel to or sole down asymptotically in the Moho. However, some reflectors are truncated by the Moho, as the one depicted in Figure 12b between CDPs 6500 and 6000. The neighboring IBERSEIS seismic profile (Figure 1b) displays a similar Moho, with a flat attitude independently of inferred Variscan orogenic roots [*Simancas et al.*, 2003]. Accordingly, the sub-horizontal Moho in the IBERSEIS and ALCUDIA transects of SW Iberia must be a post-orogenic feature, though its age is ill constrained. If a significant thermal re-equilibration or magmatic underplating is needed to reset a Moho [*Cook et al.*, 2010], the resetting time would have been most probably the Permian. On the contrary, slow re-equilibration of the crust attending mainly to isostatic and tectonic reasons would have also resulted in a horizontal Moho, which would be post-Permian in that case.

5.3. Tectonic Shortening at Different Crustal Levels

[45] Orogenic shortening is easily recognized near the edges of colliding plates. Suture zones allow the lower crust to sink/underplate into the mantle, thus compensating upper crustal shortening. A nearby example is the SPZ and OMZ structures described by *Simancas et al.* [2003] for the IBERSEIS profile (Figure 1). However, intracontinental areas are challenging in the study of shortening accommodation at different crustal levels. In this regard, the ALCUDIA profile is an opportunity to elucidate how deformation affects the whole crust in intracontinental areas far away from suture zones (e.g., ECORS [*ECORS Pyrenean Team*, 1988], LITHOPROBE [*Cook et al.*, 1999]). The issue is especially important in this part of the

CIZ, where relatively simple surface geology only allows geometrical projection of the deformational structures down to 4–5 km. The Variscan folds and thrusts observed in most of the upper crust of the ALCUDIA transect represent moderate shortening in relatively simple trains of kilometer-scale upright folds of Late Carboniferous age (D3) (Figures 2 and 4). The only remarkable exception to this statement is the southern end of the transect, adjacent to the boundary with the OMZ, that has undergone a more protracted evolution including Devonian recumbent folds (D1), Mississippian extension (D2) and, finally, Late Carboniferous shortening affecting the whole transect (D3; Figures 11a and 11b).

[46] In the central segment of the ALCUDIA profile, the upper crustal Variscan shortening seems to have no counterpart in the mid-lower crust, where there are no identified shortening structures (Figure 5d). Conversely, the northern and southern segments of the ALCUDIA profile show conspicuous shortening structures in the lower crust (Figure 5d). Thus, whereas the upper crust has homogeneously distributed shortening along the transect, the lower crust has concentrated it in two sectors. Therefore, a decoupling zone in coincidence with the top of the reflective mid-lower crust is needed. Such features were obtained in experiments on shortening of layered analogue models that incorporate the vertical heterogeneity and anisotropy of a continental lithosphere containing discontinuities, in particular the brittle/ductile rheological stratification of crustal materials [*Davy and Cobbold*, 1991; *Burg et al.*, 1994]. These experiments illustrate, among others, (1) major thrust sheets corresponding to prism-shaped seismic structures, (2) decoupled upper/lower crustal layers, and (3) lower crustal imbricated thrusts involving upper mantle rocks.

[47] The northern end of the profile shows a prominent thrust affecting the lower crust. The geometry previously described (section 4.3) allows identifying the ramp in the hanging wall and in the footwall, in order to evaluate ca. 35 km of thrust displacement (Figure 8). Moreover, the footwall ramp makes the thrust to climb from 8.5 to 6.5 s, implying a crustal thickening of 2 s (i.e. ~6 km) correlatable with the upward displacement of the top of the reflective crust, which at the northern end of the profile is at 3 s (~8 km depth) (Figure 5). At surface, this contractional structure should have created a positive relief, which has been modeled in Figure 8. In close coincidence, two normal faults (TF and MF) have been imaged, suggesting gravitational instability. Normal faulting may have been triggered by rheological weakening due to coeval granite magmatism (the Mora pluton).

[48] The southern segment of the ALCUDIA profile shows a crust-mantle wedge affecting again the mid-lower crust (section 4.4). The wedge (crocodile) geometry yields ~30 km of shortening (Figure 11b). Considering the climb of the lower crustal thrust (from 9.5 to 7 s), the crustal thickening caused by this thrust is of ~2.5 s (i.e. ~7–8 km). The wedge is located underneath the prominent D2 Pedroches Mississippian sedimentary basin (Figure 11a). Thus, D3 Late Carboniferous crustal thickening affected a previously extended and subsided crust, which has been folded in an anticlinal structure above the wedge (Figure 11b). Furthermore, the crustal thickening approximately compensates the estimated Mississippian subsidence (≥6000 m) [*Martínez Poyatos et al.*, 2001a]. Another wedge structure in the lower crust was imaged 50 km to the northwest in the IBERSEIS profile (Figures 1 and 11c) [*Simancas et al.*, 2003]. These two wedges correlate laterally along the regional structural trend, though they show opposite vergences (Figure 11c). The lateral change between these wedges, if connected, suggests the existence of a transfer fault in between, indicating how complex the 3D geometry of the lower crust can be. The IBERSEIS wedge also originated a culmination that affects conspicuous mid-crustal reflectors, while at surface it may have contributed to the structural dome with Alcudian rocks that crop out in the Castuera area (Figure 2a) [*Díez Balda et al.*, 1990].

[49] To sum up, two major structures in the lower crust accumulate a shortening of ~65 km which for the length of the ALCUDIA profile (230 km), thus representing ~23% shortening of the lower crust. Shortening in the decoupled upper crust is more regularly distributed and difficult to evaluate. However, taking into account the style of folding (Figure 2), it should be of the same order. Thus, considering the CIZ portion covered by the ALCUDIA transect, the orogenic shortening seems to be equally compensated in the upper and the lower crust, though the way that shortening is accommodated is dramatically different in each case. Our study supports the results of comparable analogue models, for example the deformation experiments of *Brun* [2002] on multilayer models simulating simplified strength profiles of a lithosphere with brittle (frictional) and ductile (viscous) rheologies. These experiments demonstrated that the coupling/decoupling between brittle and ductile layers play a dominant role on localized versus distributed deformation.

6. Conclusions

[50] The ALCUDIA deep seismic reflection transect, acquired using the Vibroseis seismic technique, is a 230 km long, high-resolution profile that samples a representative crustal section of an intracontinental orogenic domain in the southern Central Iberian Zone of the Variscan Belt. The transect constitutes the northward prolongation of the previous IBERSEIS transect, which sampled the sutures between the South Portuguese, Ossa-Morena and Central Iberian zones.

[51] The processed ALCUDIA seismic image shows a clear Moho discontinuity at 10 s TWTT (~30 km depth) that overlies an almost seismic transparent mantle down to 20 s (~70 km depth). The weakly reflective upper crust contrasts with a high-amplitude strongly reflective mid-lower crust. These two levels of contrasting reflectivity suggest the existence of a decoupling zone in between. It also suggests the existence of important lithological/rheological variations that have led to different deformation processes in both parts of the crust. North- and south-dipping reflections in the upper crust image folds and faults that branch out of the decoupling zone at 4–5 s (~11–14 km depth).

[52] The ALCUDIA transect can be divided in three segments (northern, central and southern) according to the structures identified in the lower crust. The different styles of deformation featured in each segment, together with the surface geology, help to understand the accommodation of deformation in intracontinental orogenic areas.

[53] In the central segment, the lower crust does not display major evidences for shortening, the seismic reflectivity

being subhorizontal and slightly braided. In the northern segment, a prominent flat-ramp-flat geometry is interpreted as a south-vergent thrust structure. Recognition of the footwall and hanging wall ramp terminations yields ~35 km of displacement and ~2 s (~6 km) of thickening along the section. The thickening might have developed a culmination above, which collapsed by extensional faults to recuperate normal crust thickness.

[54] The most outstanding feature on the ALCUDIA seismic image is a complete crocodile-shaped lower crust tectonic wedge that also involves the upper mantle, below the Pedroches area in the southern segment of the transect. The shortening is estimated here to be ~30 km, causing a crustal thickening of ~2.5 s (~7–8 km) that inverted and folded the overlying Mississippian Pedroches Basin.

[55] Considering each segment independently, the shortening estimated from surface geology does not fit that obtained from the seismic image for the lower crust, although the deformation accommodated by ductile deformation of the lower crust cannot be calculated. This discrepancy may be due to mid-crustal decoupling. Since upper and lower crust shortening seems to balance over the whole ALCUDIA transect, the displacement on the mid-crustal detachment should be limited. Rheological differences produced distributed deformation in the upper crust and localized thrust structures in the lower crust.

[56] **Acknowledgements.** Funding for the field acquisition of the ALCUDIA transect has been provided by the Spanish Ministry of Science and Innovation (grants: CGL2004-04623/BTE, CGL2007-63101/BTE, CGL2011-24101, CSD2006-00041) and the Junta de Castilla-La Mancha. Logistic help has also been provided by the Instituto Geológico y Minero de España. The transect has been acquired by an academic crew, whose enthusiastic work in hard weather conditions has been essential for the accomplishment of this project. It is composed of J. Álvarez, J. Álvarez-Marrón, F. Anahnah, P. Ayarza, J. M. Azañón, A. Azor, D. Brown, G. Buffett, Á. Cañamero, R. Carbonell, I. Corral, E. M. Fernández Fernández, B. Gaite, J. Galindo-Zaldívar, J. L. Gallardo Millán, J. L. García Lobón, A. González, P. González Cuadra, F. González Lodeiro, L. Guasch, P. Ibarra, A. Jabaloy, A. Jiménez, I. Jiménez Munt, J. M. Llorente, S. Lorenzo, J. Luengo, L. Mansilla, L. M. Martín Parra, P. Martínez García, D. Martínez Poyatos, J. Matas, F. Palero, I. Palomeras, A. Pedrera, A. Pérez-Estaún, S. Pérez Hernández, J. Rodríguez, M. J. Rodríguez Peces, P. Ruano, A. Ruiz-Constán, G. Santos Delgado, J. F. Simancas, J. I. Soto, and R. Tejero. We also thank the field crew of our contractor CGG for their assistance during the acquisition. We are indebted to J.-P. Burg and D. Gapais for their valuable comments and suggestions.

References

Allmendinger, R. W., T. A. Hauge, E. Hauser, C. J. Potter, S. L. Klemperer, K. D. Nelson, P. Knuepfer, and J. Oliver (1987), Overview of the COCORP 40°N Transect, western United States: The fabric of an orogenic belt, *Geol. Soc. Am. Bull.*, *98*(3), 308–319, doi:10.1130/0016-7606(1987)98<308:OOTCNT>2.0.CO;2.

Andonaegui, P. (1990), Geoquímica y geocronología de los granitoides al sur de Toledo, PhD thesis, 357 pp, Univ. Complutense, Madrid.

Arenas, R., J. R. Martínez Catalán, S. Martínez Sánchez, J. Fernández Suárez, P. Andonaegui, and J. A. Pearce (2007), The Vila de Cruces ophiolite: A remnant of the early Rheic Ocean in the Variscan suture of Galicia (northwest Iberian Massif), *J. Geol.*, *115*(2), 129–148, doi:10.1086/510645.

Ayarza, P., J. R. Martínez Catalán, J. Gallart, J. A. Pulgar, and J. J. Dañobeitia (1998), Estudio Sísmico de la Corteza Ibérica Norte 3.3: A seismic image of the Variscan crust in the hinterland of the NW Iberian Massif, *Tectonics*, *17*(2), 171–186, doi:10.1029/97TC03411.

Ayarza, P., J. R. Martínez Catalán, J. Alvarez-Marrón, H. Zeyen, and C. Juhlin (2004), Geophysical constraints on the deep structure of a limited ocean-continent subduction zone at the North Iberian Margin, *Tectonics*, *23*, TC1010, doi:10.1029/2002TC001487.

Azor, A., F. González Lodeiro, and J. F. Simancas (1994), Tectonic evolution of the boundary between the Central Iberian and Ossa-Morena zones (Variscan Belt, SW Spain), *Tectonics*, *13*, 45–61, doi:10.1029/93TC02724.

Azor, A., D. Rubatto, J. F. Simancas, F. González Lodeiro, D. Martínez Poyatos, L. M. Martín Parra, and J. Matas (2008), Rheic Ocean ophiolitic remnants in Southern Iberia questioned by SHRIMP U-Pb zircon ages on the Beja-Acebuches amphibolites, *Tectonics*, *27*, TC5006, doi:10.1029/2008TC002306.

Barbero, L. (1995), Granulite-facies metamorphism in the Anatectic Complex of Toledo, Spain: Late hercynian tectonic evolution by crustal extension, *J. Geol. Soc.*, *152*(2), 365–382, doi:10.1144/gsjgs.152.2.0365.

Braid, J. A., J. B. Murphy, C. Quesada, and J. Mortensen (2011), Tectonic escape of a crustal fragment during the closure of the Rheic Ocean: U-Pb detrital zircon data from the Late Palaeozoic Pulo do Lobo and South Portuguese zones, southern Iberia, *J. Geol. Soc.*, *168*, 383–392, doi:10.1144/0016-76492010-104.

Brown, L. D., C. J. Ando, S. L. Klemperer, J. E. Oliver, S. Kaufman, B. L. Walsh, T. Czuchra, and Y. W. Isachsen (1983), Adirondack-Appalachian Crustal Structure: The COCORP Northeast Traverse, *Geol. Soc. Am. Bull.*, *94*, 1173–1184, doi:10.1130/0016-7606(1983)94<1173:ACSTCN>2.0.CO;2.

Brun, J.-P. (2002), Deformation of the continental lithosphere: Insights from brittle-ductile models, in *Deformation Mechanisms, Rheology and Tectonics: Current Status and Future Perspectives*, edited by S. De Meer et al., *Geol. Soc. Spec. Publ.*, *200*, 355–370, doi:10.1144/GSL.SP.2001.200.01.20.

Burg, J.-P., M. Iglesias, P. Laurent, P. Matte, and A. Ribeiro (1981), Variscan intracontinental deformation: The Coimbra-Córdoba Shear Zone (SW Iberian Peninsula), *Tectonophysics*, *78*, 161–177, doi:10.1016/0040-1951(81)90012-3.

Burg, J.-P., P. Davy, and J. Martinod (1994), Shortening of analogue models of the continental lithosphere: New hypothesis for the formation of the Tibetan plateau, *Tectonics*, *13*(2), 475–483, doi:10.1029/93TC02738.

Carbonell, R., A. Pérez-Estaún, J. Gallart, J. Díaz, S. Kashubin, J. Mechie, R. Stadtlander, A. Schulze, J. H. Knapp, and A. Morozov (1996), Crustal root beneath the Urals: wide-angle seismic evidence, *Science*, *274*, 222–224, doi:10.1126/science.274.5285.222.

Carbonell, R., D. Lecerf, M. Itzin, J. Gallart, and D. Brown (1998), Mapping the Moho beneath the Southern Urals with wide-angle reflections, *Geophys. Res. Lett.*, *25*(22), 4229–4232, doi:10.1029/1998GL900107.

Carbonell, R., J. Gallart, A. Pérez-Estaún, J. Díaz, S. Kashubin, J. Mechie, F. Wenzel, and J. H. Knapp (2000), Seismic wide-angle constraints on the crust of the southern Urals, *J. Geophys. Res.*, *105*(B6), 13,755–13,777, doi:10.1029/2000JB900048.

Carbonell, R., J. Gallart, and A. Pérez-Estaún (2002), Modelling and imaging the Moho transition: the case of the southern Urals, *Geophys. J. Int.*, *149*, 134–148, doi:10.1046/j.1365-246X.2002.01623.x.

Carbonell, R., J. F. Simancas, C. Juhlin, J. Pous, A. Pérez-Estaún, F. González Lodeiro, G. Muñoz, W. Heise, and P. Ayarza (2004), Geophysical evidence of a mantle derived intrusion in SW Iberia, *Geophys. Res. Lett.*, *31*, L11601, doi:10.1029/2004GL019684.

Cook, F. A. (2002), Fine structure of the continental reflection Moho, *Geol. Soc. Am. Bull.*, *114*(1), 64–79, doi:10.1130/0016-7606(2002)114<0064:FSOTCR>2.0.CO;2.

Cook, F. A., D. S. Albaugh, L. D. Brown, S. Kaufman, J. E. Oliver, and R. D. Hatcher (1979), Thin skinned tectonics in the crystalline southern Appalachians. COCORP Seismic Reflection profiling of the Blue Ridge and Piedmont, *Geology*, *7*(12), 563–567, doi:10.1130/0091-7613(1979)7<563:TTITCS>2.0.CO;2.

Cook, F. A., A. J. van der Velden, and K. W. Hall (1999), Frozen subduction in Canada's Northwest Territories: Lithoprobe deep lithospheric reflection profiling of the western Canadian Shield, *Tectonics*, *18*, 1–24, doi:10.1029/1998TC900016.

Cook, F. A., D. J. White, A. G. Jones, D. W. S. Eaton, J. Hall, and R. M. Clowes (2010), How the crust meets the mantle: Lithoprobe perspectives on the Mohorovičić discontinuity and crust-mantle transition, *Can. J. Earth Sci.*, *47*(4), 315–351, doi:10.1139/EE09-076.

Culshaw, N. G., C. Beaumont, and R. A. Jamieson (2006), The orogenic suprastructure-infraestructure concept: Revisited, quantified and revived, *Geology*, *34*, 733–737, doi:10.1130/G22793.1.

Davy, P., and P. Cobbold (1991), Experiments on shortening of a 4-layer model of the continental lithosphere, *Tectonophysics*, *188*, 1–25, doi:10.1016/0040-1951(91)90311-F.

DEKORP Research Group (1985), First results and preliminary interpretation of deep-reflection seismic recording along profile DEKORP 2-South, *J. Geophys.*, *57*, 137–165.

DEKORP Research Group (1988), Results of the DEKORP 4/KTB Oberpfalz deep seismic reflection investigations, *J. Geophys.*, *62*, 69–101.

Díez Balda, M. A., R. Vegas, and F. González Lodeiro (1990), Central-Iberian Zone. Autochthonous Sequences. Structure, in *Pre-Mesozoic Geology of Iberia*, edited by R. D. Dallmeyer and E. Martínez García, pp. 172–188, Springer, Berlin.

Echtler, H. P., M. Stiller, F. Steinhoff, C. Krawczyk, A. Suleimanov, V. Spiridonov, J. H. Knapp, Y. Menshikov, J. Álvarez-Marrón, and N. Yunusov (1996), Preserved collisional crustal structures of the Southern Urals revealed by vibroseis profiling, *Science*, *274*, 224–226, doi:10.1126/science.274.5285.224.

ECORS Pyrenean Team (1988), The ECORS deep reflection seismic survey across the Pyrenees, *Nature*, *331*, 508–511, doi:10.1038/331508a0.

Franke, W. (2000), The mid-European segment of the Variscides: tectonostratigraphic units, terrane boundaries and plate tectonic evolution, in *Orogenic Processes: Quantification and Modelling in the Variscan Belt*, edited by W. Franke et al., *Geol. Soc. Spec. Publ.*, *179*, 35–61, doi:10.1144/GSL.SP.2000.179.01.05.

Freeman, B., S. L. Klemperer, and R. W. Hobbs (1988), The deep structure of the northern England and the Iapetus suture zone from BIRPS deep seismic reflection profiling, *J. Geol. Soc.*, *145*, 727–740, doi:10.1144/gsjgs.145.5.0727.

Friberg, M., D. Juhlin, M. Beckholmen, G. A. Petrov, and A. G. Green (2002), Palaeozoic tectonic evolution of the Middle Urals in the light of the ESRU seismic experiments, *J. Geol. Soc.*, *159*(3), 295–306, doi:10.1144/0016-764900-189.

Gebrande, H., E. Lüschen, B. Lammerer, and O. Oncken (2001), European orogenic processes-research transects the Eastern Alps, *Eos Trans. AGU*, *82*(40), 453, doi:10.1029/01EO00269.

Gómez-Pugnaire, M. T., A. Azor, J. M. Fernández Soler, and V. López Sánchez-Vizcaíno (2003), The amphibolites from the Ossa-Morena/Central Iberian Variscan suture (southwestern Iberian Massif): Geochemistry and tectonic interpretation, *Lithos*, *68*(1–2), 23–42, doi:10.1016/S0024-4937(03)00018-5.

Griffin, W. L., and S. Y. O'Reilly (1987), Is the continental Moho the crust-mantle boundary?, *Geology*, *15*(3), 241–244, doi:10.1130/0091-7613(1987)15<241:ITCMTC>2.0.CO;2.

Hammer, P. T. C., and R. N. Clowes (1997), Moho reflectivity patterns—A comparison of Canadian LITHOPROBE transects, *Tectonophysics*, *269*(3–4), 179–198, doi:10.1016/S0040-1951(96)00164-3.

Hernández Enrile, J. L. (1991), Extensional tectonics of the Toledo ductile-brittle sheaar zone, central Iberian Massif, *Tectonophysics*, *191*(3–4), 311–324, doi:10.1016/0040-1951(91)90064-Y.

Hynes, A., and D. B. Snyder (1995), Deep-crustal mineral assemblages and potential for crustal rocks below the Moho in the Scottish Caledonides, *Geophys. J. Int.*, *123*(2), 323–339, doi:10.1111/j.1365-246X.1995.tb06857.x.

Juhlin, C., M. Friberg, H. P. Echtler, T. Hismatulin, A. Rybalka, A. G. Green, and J. Ansorge (1998), Crustal structure of the Middle Urals: results from the ESRU experiments, *Tectonics*, *17*(5), 710–725, doi:10.1029/98TC02762.

Julivert, M., M. Fontboté, A. Ribeiro, and L. E. Conde (1972), *Mapa y Memoria Explicativa del Mapa Tectónico de la Península Ibérica y Baleares*, scale 1:1,000,000, 113 pp., Inst. Geol. y Min. de Esp., Madrid.

Julivert, M., J. M. Vegas, J. M. Roiz, and A. Martínez Rius (1983), La estructura de la parte SE de la Zona Centroibérica, con metamorfismo de bajo grado, in *Geología de España, Libro Jubilar de J. M. Ríos*, edited by J. A. Comba, pp. 477–489, Inst. Geol. y Min. de Esp., Madrid.

Klemperer, S. L., and D. H. Matthews (1987), Iapetus Suture located beneath the North Sea by BIRPS deep seismic reflection profiling, *Geology*, *15*, 195–198, doi:10.1130/0091-7613(1987)15<195:ISLBTN>2.0.CO;2.

Klemperer, S. L., T. A. Hauge, E. C. Hauser, J. E. Oliver, and C. J. Potter (1986), The Moho in the northern Basin and Range Province, Nevada, along the COCORP 40°N seismic-reflection transect, *Geol. Soc. Am. Bull.*, *97*, 603–618, doi:10.1130/0016-7606(1986)97<603:TMITNB>2.0.CO;2.

Lotze, F. (1945), Zur gliederung der Variszichen der Iberischen Meseta, *Geotekton. Forsch.*, *6*, 78–92.

Martínez Catalán, J. R., et al. (1995), Results from the ESCI-N3.3 marine deep seismic profile along the Cantabrian continental margin, *Rev. Soc. Geol. Esp.*, *8*, 341–354.

Martínez Poyatos, D. (2002), *Estructura del borde meridional de la Zona Centroibérica y su relación con el contacto entre las Zonas Centroibérica y de Ossa-Morena*, *Lab. Xeol. Laxe, Ser. Nova Terra*, vol. 18, 295 pp., Do Castro, Coruña, Spain.

Martínez Poyatos, D., J. F. Simancas, A. Azor, and F. González Lodeiro (1998), Evolution of a Carboniferous piggyback basin in the southern Central Iberian Zone (Variscan Belt, SE Spain), *Bull. Soc. Geol. Fr.*, *169*, 573–578.

Martínez Poyatos, D., F. González Lodeiro, A. Azor, and J. F. Simancas (2001a), La estructura de la Zona Centroibérica en la región de Los Pedroches (Macizo Ibérico meridional), *Rev. Soc. Geol. Esp.*, *14*, 147–160.

Martínez Poyatos, D., F. Nieto, A. Azor, and J. F. Simancas (2001b), Relationships between very low-grade metamorphism and tectonic deformation: Examples from the southern Central Iberian Zone (Iberian Massif, Variscan Belt), *J. Geol. Soc.*, *158*, 953–968, doi:10.1144/0016-764900-206.

Martín Parra, L. M., F. González Lodeiro, D. Martínez Poyatos, and J. Matas (2006), The Puente Genave-Castelo de Vide shear zone (southern Central Iberian Zone, Iberian Massif): geometry, kinematics and regional implications, *Bull. Soc. Geol. Fr.*, *177*(4), 191–202, doi:10.2113/gssgfbull.177.4.191.

Matte, P. (2001), The Variscan collage and orogeny (480–290 Ma) and the tectonic definition of the Amorica microplate: A review, *Terra Nova*, *13*, 122–128, doi:10.1046/j.1365-3121.2001.00327.x.

McCarthy, J., and G. A. Thompson (1988), Seismic imaging of extended crust with emphasis on the western United States, *Geol. Soc. Am. Bull.*, *100*(9), 1361–1374, doi:10.1130/0016-7606(1988)100<1361:SIOECW>2.3.CO;2.

Meissner, R. (1999), Terrane accumulation and collapse in central Europe: seismic and rheological constraints, *Tectonophysics*, *305*(1–3), 93–107, doi:10.1016/S0040-1951(99)00016-5.

Mooney, W. D., and R. Meissner (1992), Multi-genetic origin of crustal reflectivity: A review of seismic reflection profiling of the continental lower crust and Moho, in *Continental Lower Crust*, edited by D. M. Fountain, R. Arculus, and R. W. Kay, pp. 179–200, Elsevier, Amsterdam.

Onken, O., A. Plesh, J. Weber, W. Ricken, and S. Schrader (2000), Passive margin detachment during arc-continent collision (central European Variscides), in *Orogenic Processes: Quantification and Modelling in the Variscan Belt*, edited by W. Franke et al., *Geol. Soc. Spec. Publ.*, *179*, 9–20.

Ordóñez Casado, B. (1998), Geochronological studies of the Pre-Mesozoic basement of the Iberian Massif: the Ossa-Morena Zone and the Allochthonous Complexes within the Central Iberian Zone, PhD thesis, 235 pp., ETH Zurich, Zurich, Switzerland.

Ortega Gironés, E. (1986), Geology and metallogeny of the Almadén area, Centro-Iberian Zone, Spain, in *Remote Sensing in Mineral Exploration*, edited by V. Wambeke, *EEC. Rep. 11317*, pp. 147–173, Eur. Econ. Comm., Brussels.

Palomeras, I., R. Carbonell, I. Flecha, J. F. Simancas, P. Ayarza, J. Matas, D. Martínez Poyatos, A. Azor, F. González Lodeiro, and A. Pérez-Estaún (2009), Nature the lithosphere across the Variscan orogen of SW Iberia: Dense wide-angle seismic reflection data, *J. Geophys. Res.*, *114*, B02302, doi:10.1029/2007JB005050.

Palomeras, I., R. Carbonell, P. Ayarza, D. Martí, D. Brown, and J. F. Simancas (2011), Shear wave modeling and Poisson's ratio in the Variscan Belt of SW Iberia, *Geochem. Geophys. Geosyst.*, *12*, Q07008, doi:10.1029/2011GC003577.

Pereira, M. F., J. B. Silva, K. Drost, M. Chichorro, and A. Apraiz (2010), Relative timing of transcurrent displacements in northern Gondwana: U-Pb laser ablation ICP-MS zircon and monazite chronology of gneisses and sheared granites from the western Iberian Massif (Portugal), *Gondwana Res.*, *17*, 461–481, doi:10.1016/j.gr.2009.08.006.

Pérez-Estaún, A., J. R. Martínez Catalán, and F. Bastida (1991), Crustal thickenning and deformation sequence in the football to the suture of the Hercynian Belt of NW Spain, *Tectonophysics*, *191*, 243–253, doi:10.1016/0040-1951(91)90060-6.

Pérez-Estaún, A., J. A. Pulgar, E. Banda, J. Álvarez-Marrón, and the ESCI-N Research Group (1994), Crustal structure of the external variscides in northern Spain from deep seismic reflection profiling, *Tectonophysics*, *232*, 91–118, doi:10.1016/0040-1951(94)90078-7.

Pérez-Estaún, A., J. A. Pulgar, J. Álvarez-Marrón, and the ESCI-N Group (1995), Crustal structure of the Cantabrian Zone: seismic image of a Variscan foreland thrust and fold belt (NW Spain), *Rev. Soc. Geol. Esp.*, *8*, 307–320.

Pous, J., et al. (2011), Constraints on the crustal structure of the internal Variscan Belt in SW Europe: A magnetotelluric transect along the eastern part of Central Iberian Zone, Iberian Massif, *J. Geophys. Res.*, *116*, B02103, doi:10.1029/2010JB007538.

Pulgar, J. A., A. Pérez-Estaún, J. Gallart, J. Álvarez-Marrón, J. Gallastegui, J. L. Alonso, and the ESCI-N Group (1995), The ESCIN-2 deep seismic reflection profile: a traverse across the Cantabrian Mountains and adjacent Duero basin, *Rev. Soc. Geol. Esp.*, *8*, 383–394.

Robardet, M. (2002), Alternative approach to the Variscan Belt in southwestern Europe: Preorogenic paleobiogeographical constraints, in *Variscan-Appalachian Dynamics: The building of the Late Paleozoic Basement*, edited by J. R. Martínez Catalán et al., *Spec. Pap. Geol. Soc. Am.*, *364*, 1–15.

Rodríguez-Alonso, M. D., M. Peinado, M. López-Plaza, P. Franco, A. Carnicero, and J. C. Gonzalo (2004), Neoproterozoic-Cambrian synsedimentary magmatism in the Central Iberian Zone (Spain): geology, petrology and geodynamic significance, *Int. J. Earth Sci.*, *93*(5), 897–920, doi:10.1007/s00531-004-0425-4.

Schmelzbach, C., C. Juhlin, R. Carbonell, and J. F. Simancas (2007), Prestack and poststack migration of crooked-line seismic reflection data: A

case study from the South Portuguese Zone fold belt, southwestern Iberia, *Geophysics*, *72*(2), 9–18, doi:10.1190/1.2407267.

Simancas, J. F., et al. (2003), The crustal structure of the transpresional Variscan Orogen of the SW Iberia: The IBERSEIS Deep Seismic Reflection Profile, *Tectonics*, *22*(6), 1062, doi:10.1029/2002TC001479.

Smithson, S. B. (1989), Contrasting types of lower crust, in *Properties and Processes of Earth's Lower Crust*, *Geophys. Monogr. Ser*, vol. 51, edited by R. F. Mereu, S. Mueller, and D. M. Fountain, pp. 53–63, AGU, Washington, D. C., doi:10.1029/GM051p0053.

Tait, J., M. Schätz, V. Bachtadse, and H. Soffel (2000), Palaeomagnetism and Palaeozoic palaeogeography of Gondwana and European terranes, in *Orogenic Processes: Quantification and Modelling in the Variscan Belt*, edited by W. Franke et al., *Geol. Soc. Spec. Publ.*, *179*, 21–34, doi:10.1144/GSL.SP.2000.179.01.04.

Tryggvason, A., D. Brown, and A. Pérez-Estaún (2001), Crustal architecture of the southern Uralides from true amplitude processing of the URSEIS vibroseis profile, *Tectonics*, *20*, 1040–1052, doi:10.1029/2001TC900020.

Vidal, G., S. Jensen, and T. Palacios (1994), Neoproterozoic (Vendian) ichnofossils from Lower Alcudian strata in central Spain, *Geol. Mag.*, *131*, 169–179, doi:10.1017/S0016756800010700.

Yilmaz, O. (2001), *Seismic Data Analysis*, *Invest. Geophys.*, vol. 10, edited by S. M. Doherty, 2027 pp., Soc. of Explor. Geophys., Tulsa, Okla.